Single-cell proteomics and transcriptomics capture eosinophil development and identify the role of IL-5 in their lineage transit amplification

Joseph Jorssen, MSc[1,*], Glenn Van Hulst, MSc[1,*], Kiréna Mollers, MSc[1], Julien Pujol, DVM, PhD[1], Georgios Petrellis[2], DVM, Antonio P. Baptista, DVM, PhD[3,4], Sjoerd Schetters, PhD[3,4], Frédéric Baron, MD, PhD[5], Jo Caers, MD, PhD[5], Bart N.Lambrecht, MD, PhD[3,4,6], Benjamin G. Dewals[2], DVM, PhD[2], Fabrice Bureau, DVM, PhD[1,*], Christophe J. Desmet, PhD[1,*]

[1] Laboratory of Cellular and Molecular Immunology, GIGA Institute, Faculty of Veterinary Medicine, University of Liege, B34 Avenue de l'Hopital 1, B4000 Liege, Belgium

[2] Laboratory of Parasitology, FARAH Institute, University of Liege, Faculty of Veterinary Medicine, Avenue de Cureghem 10, B4000 Liège, Belgium.

[3] Laboratory of Immunoregulation and Mucosal Immunology, VIB-UGent Center for Inflammation Research, Ghent, Belgium

[4] Department of Internal Medicine and Pediatrics, Ghent University, Ghent, Belgium

[5] Laboratory of Haematology, GIGA Institute, Faculty of Medicine, Liege University Hospital Centre, University of Liege, B34 Avenue de l'Hopital 1, B4000 Liege, Belgium

[6] Department of Pulmonary Medicine, Erasmus MC, Rotterdam, Netherlands

[*]Equal contributors

Lead Contact footnote: Christophe J. Desmet, PhD, Laboratory of Cellular and Molecular Immunology, GIGA Institute, University of Liege, B34, 1 Avenue de l'Hopital, B4000 Liege, Belgium. Phone: +3243663708, Fax: +3243664198, email: christophe.desmet@uliege.be

Corresponding author email: christophe.desmet@uliege.be

Summary

The activities, ontogeny, and mechanisms of lineage expansion of eosinophils are less well-resolved than those of other immune cells, despite the use of biological therapies targeting the eosinophilia-promoting cytokine IL-5 or its receptor IL-5Rα. We combined single-cell proteomics and transcriptomics and generated transgenic IL-5Rα reporter mice to revisit eosinophilopoiesis. We reconciled human and murine eosinophilopoiesis and provided extensive cell surface immunophenotyping and transcriptomes at different stages along the continuum of eosinophil maturation. We used these resources to show that IL-5 promoted eosinophil lineage expansion via transit amplification, while its deletion or neutralization did not compromise eosinophil maturation. Informed from our resources, we also showed that Interferon Response Factor-8, considered an essential promoter of myelopoiesis, was not intrinsically required for eosinophilopoiesis. This work hence provides resources, methods, and insights for understanding eosinophil ontogeny, the effects of current precision therapeutics and the regulation of eosinophil development and numbers in health and disease.

Introduction

Eosinophils are specialized granulocytes whose exact physiologic and pathophysiological activities are still not fully understood [1,2]. Initially recognized to accumulate in response to helminth infection [3], eosinophils are also increasingly acknowledged for their role in immune homeostasis [4,5], microbial defense [6–8], metabolism [9] or anticancer protection [10]. Despite their proposed beneficial functions, eosinophils are predominantly considered for their diagnostic value and implication in a broad spectrum of non-communicable diseases termed eosinophil-associated diseases (EADs) [1,2]. EADs are most often driven by type 2 immune processes, and are characterized by an accumulation of eosinophils in blood and diseased tissues. EADs include highly prevalent mucosal diseases such as eosinophilic asthma and eosinophilic chronic rhinosinusitis with nasal polyps but also less common eosinophilic vasculitis and idiopathic hypereosinophilic syndromes.

In EADs, the increased presence of circulating eosinophils, known as eosinophilia, serves as a valuable diagnostic marker and is used for treatment allocation. It is commonly assumed that blood eosinophilia primarily results from increased eosinophil production by the bone marrow (BM) [1]. The first identified eosinophil-committed hematopoietic progenitors, often called "EoPs", appeared as a subset of the heterogeneous granulocyte/monocyte progenitor pool (GMP) in mice [11], or of the common myeloid progenitor pool (CMP) in human [12]. However, the traditional perspective proposing that eosinophils share developmental proximity to all other granulocytes including neutrophils, arising from the hypothesis that the GMP and CMP represent defined oligopotent developmental stages of hematopoietic progenitors, has been invalidated. Recent studies concur in showing that myelopoiesis proceeds along 2 distinct arms; one consisting of lineages expressing the GATA1 transcription factor, which give rise to eosinophils, basophils, erythrocytes and megakaryocytes, and a separate arm that leads to the development of neutrophils and monocytes [13–17]. Therefore, previous assumptions on eosinophilopoiesis built within the framework of the GMP and CMP concepts need revision.

Due to the currently limited resolution of the eosinophil lineage, the mechanisms leading to increased eosinophil production from hematopoietic progenitors are also not well understood [18]. It is known that the cytokine interleukin (IL)-5 [19] is essential to eosinophilia, as was established first in *Il5*-deficient mice [20,21]. Alarmin cytokines such as IL-33 can also trigger eosinophilia but appear to do so indirectly by stimulating type 2 innate lymphoid cells (ILC2s) and helper T (Th2) cells, thereby increasing IL-5 production [22].

The dependency of eosinophilia on IL-5 led to the development of neutralizing anti-IL-5 monoclonal antibodies for the treatment of EADs [23,24]. These precision therapies alleviate blood eosinophilia and are used in the treatment of severe forms of EADs including severe eosinophilic asthma [25]. Cytotoxic antibodies to IL-5Rα were also developed, which deplete virtually all tissue and circulating eosinophils [26]. Other precision therapies for the treatment of EADs impact on blood eosinophil counts as well. For instance, the IL-4Rα-targeting antibody dupilumab elicits transient blood eosinophilia in a fraction of patients [27]. Alternatively, the anti-TSLP tezepelumab [28] and the anti-IL-33 itepekimab [29] both reduce blood eosinophil counts in asthmatic patients. With the current shift toward precision therapies for EADs comes the need for a refined understanding of eosinophil development and lineage expansion.

Here, we aimed to better resolve eosinophil development in human and mice. We obtained single-cell resolution of eosinophilopoiesis by combining single-cell proteomic screening by flow cytometry, generating a transgenic IL-5Rα reporter mouse strain and (single-cell) transcriptomic analyses. Our comparative analyses highlighted the evolutionarily conserved ontogeny of eosinophils, along a continuum of immunophenotypic stages of maturation in human and mice. We illustrate how these transcriptomic and immunophenotypic resources may be leveraged to investigate the molecular requirements and cellular dynamics of eosinophil progenitor maturation and expansion in eosinophilia, and to elucidate how IL-5 depletion impacts eosinophil development.

Results

Droplet-based single-cell RNA sequencing captures the first stages of eosinophilopoiesis

We first aimed to resolve the development of eosinophils starting from their first identifiable progenitors in the BM of mice, with the aim of finding tractable cell surface markers for further identification. We resorted to single-cell RNA sequencing (scRNAseq) of lineage (lin)-negative c-Kit^{+} IL-7Rα^{-} progenitors sorted from the BM of steady-state mice using a 10X droplet-based approach to generate a "snapshot" of the ontogenic relationships of early eosinophil progenitors [13,30]. Uniform Manifold Approximation and Projection (UMAP [31]) displayed the 2 major branches of myelopoiesis (Figure 1A), with one arm giving rise to monocytes and neutrophils and another arm of *Gata1*-expressing progenitors leading to the erythroid, megakaryocyte, basophil and eosinophil lineages (Figure 1B). Early eosinophil-committed progenitors were identified based on their expression of eosinophil marker genes (*Epx*, *Prg3*, …) and displayed quality of data comparable to that of other progenitors (Figure 1C, Table S1 and Figure S1A).

To zoom in on eosinophil ontogeny, we sub-selected hematopoietic stem and progenitor cells (HSPCs) clusters containing hematopoietic stem cells (HSCs, marked by the expression of the *Hlf* transcription factor [32]) and those belonging to the *Gata1*-expressing subbranch leading to the basophil/mast cell and eosinophil lineages (Figure 1B-C). UMAP of this sub-selection and Slingshot trajectory inference displayed a continuum from HSPCs toward eosinophil/basophil/mast cell (EBM) progenitors, which in turn separated into basophil - committed and eosinophil-committed progenitors identifiable by lineage marker genes such as *Cd200r3* and *Epx*, respectively (Figure 1D-F). We did not detect progenitors with specific mast cell markers different from markers also shared with basophils, possibly owing to the rarity of mast cells in normal murine BM. Previous scRNAseq analyses on larger number of progenitors identified putative mast cell progenitors in murine BM, which were proposed to share a common progenitor pool with basophils [33]. Based on this current hypothesis, we postulate that EBM clusters identified here likely encompassed progenitors of both basophils and BM-derived mast cells, but we will not refer to mast cells in subsequent analyses of our scRNAseq dataset.

We then used single-cell regulatory network inference and clustering (SCENIC) [34] to position the activity of key transcription factors involved in eosinophilopoiesis in this

actualized developmental path. We observed 4 major patterns among regulons. The first cluster consisted in regulons of transcription factors associated with HSCs such as HLF (Figure S1B). A second cluster displayed upregulated activity of transcription factors in EBM progenitors, which included GATA1 and GATA2, consistent with their belonging to the "GATA1" arm of myelopoiesis. EBM progenitors also upregulated the activity of transcription factors involved in endoplasmic reticulum homeostasis including XBP1, which is particularly important for eosinophil maturation [35]. A third cluster of transcription factors involved in terminal myeloid cell maturation and function was upregulated in basophil progenitors. This cluster also contained C/EBPα, which was already upregulated in EBM progenitors, in line with its role in basophil and eosinophil differentiation [18]. Finally, eosinophil commitment was characterized by a small cluster of regulons mostly displaying upregulation of C/EBPε, a known promoter of eosinophil differentiation [36]. Eosinophil differentiation also involved the downregulation of C/EBPα activity, consistent with the required balance between C/EBPα and C/EBPε for normal eosinophil development [37]. One unexpected observation was the low activity of Interferon response factor-8 (IRF8) along eosinophil ontogeny (Figure S1B), since IRF8 has been proposed to play an important role in eosinophil differentiation, maturation and expansion [18,38].

Within this actualized transcriptomic landscape of eosinophilopoiesis, we finally aimed to find cell surface markers of early eosinophil progenitors. Noticeably, *Il5ra* gene expression was detectable in the first identifiable eosinophil progenitors, but not earlier (Figure S1C). Aside from *Il5ra*, we did not identify detectable or discriminating expression of other cell surface markers, including *Siglecf*, *Adgre1* (encoding F4/80), or *Ccr3* (Table S1 and Figure S1C). The earliest identifiable eosinophil progenitors in mice hence might be best defined by exclusion of other lineages.

Single-cell RNA sequencing is limited for resolving eosinophil maturation

We next evaluated whether different automated methods of scRNAseq could be implemented to identify cell surface markers resolving eosinophil maturation downstream of lineage commitment. We reanalyzed a recently published dataset of well-based scRNAseq on Siglec-F^+ BM cells from highly eosinophilic IL-5 transgenic mice [8]. Using a recommended resolution in Seurat returned 4 clusters of eosinophil lineage cells in the BM of these mice, which differed by their expression of genes associated with eosinophil function (*Epx, Ccr3,* ...) and the cell

cycle (*Mki67, Top2a, ...*) (Figure S2A). Complicating the analysis, no differential expression of cell surface marker genes could be detected that discriminated the different clusters of eosinophils from each other, except for a putatively more mature *Ccr3*-expressing subset (Table S2). We likewise performed a 10X droplet-based analysis on Siglec-F^{+} BM cells from mice rendered highly eosinophilic by repeated injections of IL-33. This method too recovered analyzable eosinophils, this time in 3 predicted clusters differing again by their expression of genes associated with eosinophil function (*Epx, Ccr3, Prg3*, …) and the cell cycle (*Pcna*, …) (Figure S2B). Yet again, only the presumably more mature eosinophil subset differentially expressed cell surface marker genes such as *Ccr3* (Table S2). Finally, we tested whether fixing cells in droplet-based 10X Flex scRNAseq could provide more RNA data in eosinophils among CD55^{+} Dump (Ly6G, B220, NK1.1, CD90.2)$^{-}$ cells of GATA1 lineages from steady-state wild-type mice. Additionally, cells were labeled with oligo-tagged antibodies to improve lineage identification and the recovery of cells with low RNA content. Combining RNA and protein information allowed the identification of the major GATA1 lineages and captured a continuum of eosinophil maturation from c-Kit^{+} CCR3^{-} to c-Kit^{-} CCR3^{hi} eosinophils along 4 putative clusters (Figure S2C-E). Nonetheless, the cellular RNA information dropped along eosinophil maturation, leading to a resolution that relied mostly on protein data. Altogether, while different platforms were able to capture eosinophils, depth of analysis and cell recovery in scRNAseq were suboptimal, especially for mature eosinophils. Reasons for this issue remain to be fully resolved but are often assumed to relate to high amounts of inhibitor-resistant RNAses in eosinophils [39].

Single-cell proteomic screening in flow cytometry resolves the maturation of murine eosinophils

Due to limitations of scRNAseq in resolving eosinophil maturation, we turned to single-cell surface proteome screening by flow cytometry, which has been previously used to resolve neutropoiesis [40]. We used our scRNAseq analyses to inform an initial backbone marker panel aimed at capturing the continuum between the earliest identifiable eosinophil progenitors among c-Kit^{+} CD55^{+} "GATA1" progenitors, and mature eosinophils known to express CCR3 and Siglec-F, while excluding other lineages (Figure S3A). We used Infinity Flow [41] to combine this panel with a large-scale flow cytometric screening for 264 surface markers (LEGENDScreen, Biolegend, Figure 1G, Figure S3B). Major cell populations were classified using lineage markers based on prior knowledge (Figure S3C and Table S3). UMAP of the

Infinity Flow output provided a consistent snapshot of the ontogenic relationships of eosinophils (Figure 1H, I). The eosinophil lineage emerged from a pool of $CD55^+$ c-Kit^+ Sca-1^+ HSPCs, from which also diverged the erythroid, megakaryocytic, mast cell and basophil lineages, while monocytes and neutrophils were excluded from this branch of myelopoiesis (Figure 1H, J). Downstream of the early divergence of $CD55^+$ GATA1 lineages, eosinophils arose together with basophils and mast cells from a pool of $CD45^+$ $CD55^+$ $CD115^-$ $CCR3^-$ $dump^-$ $CD200R3^-$ $CD11b^-$ c-Kit^{int} Sca-1^- $CD150^-$ progenitors (Figure 1H, K).

We next inspected the 132 antibodies that labelled cells of the eosinophil lineage and improved the resolution of eosinophil maturation (Table S4). UMAP of the Infinity Flow output identified a continuum of eosinophil maturation comprising 4 main immunophenotypes appearing as distinguishable density nodes. To facilitate the further characterization of eosinophil progenitors at different stages of their maturation process, we chose to partition the continuum of eosinophil maturation based on these 4 immunophenotypes, which we refer to here as stages I to IV (Figure 2A). Among the 21 antibodies delivering strong signal (background-corrected median fluorescence intensity (MFI) > 10^3) at any stage of eosinophil maturation were markers previously associated with murine eosinophil progenitors such as CD34, which became downregulated along eosinophil maturation, as well as markers of mature eosinophils and granulocytes such as CCR3/CD193 and CD11b, which were progressively upregulated (Figure 2A). We optimized our initial panel by incorporating 3 additional markers: PIR-A/B, a marker highly upregulated along eosinophil maturation (Figure 2A-D), as well as F4/80 and CD29 (also known as integrin-β1, ITGB1) as discriminating markers that help exclude contaminant cells (Figure 2B-D, Figure S3D). The resulting 9-color conventional flow cytometric panel allowed to identify and sort 4 stages of murine eosinophil maturation (Figure 2C-E). Progenitors in stages I and II displayed eosinophilic granules and large, often contorted nuclei, with central hollowing of the nucleus visible in a majority of stage II cells (Figure 2E). Cells in stage III cells were distinctively smaller than in stages I-II, and exhibited ring-shaped nuclei, while stage IV cells displayed the classical morphology of mature murine eosinophils.

Next, we aimed to characterize the relationship between these 4 stages of eosinophil development using bulk RNA-sequencing. Principal component analysis (PCA) positioned the 4 stages on a continuum along the first principal component (PC1) that captured 76% of the variance (Figure 2F). This analysis highlighted a major transcriptional transition happening between stages II and III, even though pairwise comparisons returned hundreds of differentially expressed genes (FDR<0.05) at transitions between stages I-II and III-IV (Figure 2F). We used

hierarchical clustering to identify prominent patterns of gene regulation (>100 genes/pattern) in a likelihood ratio test (LRT) identifying well-expressed genes (baseMean>100) that were differentially expressed along eosinophilopoiesis (FDR<1.10^{-4}), and tested their enrichment in Gene Ontology (GO) biological pathways. Stage I progenitors expressed on average the highest expression of genes associated with protein synthesis and ribosome biogenesis, while eosinophil granule protein-coding genes and genes associated with the cell cycle were highly expressed in both stages I and II (Figure 2G-I, Table S5). Expression of these genes decreased in stages III and IV. Stage III cells displayed higher expression of a small set of genes associated with innate immunity including eosinophil-associated RNAses. Finally, genes associated with mature myeloid cell function were progressively upregulated along eosinophil maturation, reaching their peak expression in stage IV eosinophils. The downregulation of eosinophil granule- and cell cycle-associated genes in the transition between stages II and III, along with the upregulation of myeloid function-associated genes were the most prominent transcriptomic changes along steady-state eosinophilopoiesis. The above data were consistent with cells in stage I-II being myelocytes primarily involved in eosinophil granule production and lineage expansion in the steady-state, before transitioning toward non-proliferating stage III metamyelocytes and stage IV mature eosinophils.

Single-cell proteomic screening in flow cytometry shows conservation of human and murine eosinophilopoiesis

We performed a similar surface proteome screening in healthy human BM (Figure 3A, Figure S4A). We used UMAP visualization of the Infinity Flow output and annotated major cell populations using lineage markers (Figure 3B-C, Figure S4B-C and Table S3). Confirming the robustness of the approach, a sub-analysis of neutrophil lineage cells captured 4 previously proposed stages of neutrophil maturation [40] (Figure S4D). As in mice, human eosinophils, basophils and mast cells shared a common pool of progenitors (Figure 3B, D). Of note, CD125 surface expression was upregulated in committed eosinophil progenitors compared to cells engaging toward the basophil and mast cell lineages (Figure 3D).

We then focused on eosinophil maturation and observed that the continuum of maturation of human eosinophils encompassed 4 main immunophenotypes in our analysis, similarly to mice (Figure 4A). Hence, we opted to partition the continuum of human eosinophil maturation into 4 stages as well (I to IV). To generate a conventional flow cytometric antibody panel for human eosinophil maturation, we inspected the 153 screening antibodies that stained

eosinophil lineage cells (Table S6) and focused on the 43 antibodies generating strong signal (background-corrected MFI>2.10^3) in at least one of the 4 stages of eosinophil maturation (Figure 4B). This selection contained known surface markers of human eosinophils in addition to markers not previously reported on human eosinophils such as TNFRSF12A (CD266/TWEAKR/FN14) (Figure 4B). Because of its dynamic regulation along human eosinophilopoiesis, we included CD84 into an optimized 10-color flow cytometric panel. We used this panel to isolate and study consecutive immunophenotypic stages of human eosinophil maturation (Figure 4C-E). Based on their distinctive eosinophilic granule content and nuclear shape, cells in stage I-II were eosinophilic myelocytes, whereas stage III cells were metamyelocytes and stage IV cells were mature eosinophils (Figure 4E).

Next, we sorted the above 4 stages of human eosinophil maturation from 3 healthy donors and compared their transcriptome by RNAseq. A PCA positioned these 4 stages on a continuum along PC1 that captured 71% of the variance (Figure 4F, upper). As in mice, the most prominent transcriptomic changes happened between stages II and III, even though transitions between stages I-II and III-IV involved changes in the expression of hundreds of genes (Figure 4F, lower). Three main patterns of changes of gene expression were observed along human eosinophilopoiesis (Figure 4G, Table S7). Like in mice, progenitors in stage I displayed the highest expression of genes involved in ribosome biogenesis and protein synthesis, while cells in stages I and II displayed the highest expression of eosinophil granule- and cell cycle-associated genes (Figure 4G-I). Transition to stage III metamyelocytes was accompanied by a downregulation of these genes, while the expression of myeloid function-associated genes steadily increased from stages I to IV. These analyses highlight a conserved developmental program of eosinophilopoiesis in both humans and mice, providing a basis for translational studies as well as opportunities to study shared mechanisms of eosinophil development.

Eosinophil progenitor expansion is driven by increased transit amplification

Having resolved a conserved developmental trajectory of eosinophilopoiesis, we aimed to uncover the mechanisms underlying eosinophil progenitor expansion using models of eosinophilic disease in mice. We first used a very robust model of eosinophilia with features of eosinophilic granulomatosis polyangiitis [42] consisting of daily intraperitoneal injections of IL-33 and followed changes in the maturation stages of eosinophils through time by flow cytometry (Figure 5A-D). Importantly, the immunophenotyping panel established for steady-

state eosinophilopoiesis continued to resolve 4 main immunophenotypic stages of eosinophil maturation in eosinophilic conditions (Figure S5A). Abundance of cells in maturation stages I, II and III increased over time, reaching a peak fold amplification at the end of the 7 days of IL-33 treatment (Figure 5B, C). Discontinuation of IL-33 stimulation led to a drop in the abundance of stage III progenitors, paralleled by a further increase of mature stage IV eosinophils in the BM and blood. Abundance of stage I-III progenitors returned close to baseline values within 5 days, while blood and BM mature eosinophils started to decrease.

A similar dynamic expansion of the eosinophil lineage was observed in response to subcutaneous infection with *Nippostrongylus brasiliensis* larvae. Eosinophil progenitors were expanded on day 8, the time around which the parasite is cleared in mice [43,44] (Figure 5E). Progenitor abundance returned toward a steady-state profile by day 15 post-infection, even though blood and BM mature eosinophils remained increased (Figure 5E). In a model of repeated intranasal administration of extracts of the allergenic mold *Alternaria alternata*, abundance of eosinophil lineage cells increased after 8 days of continued stimulation and returned to baseline values within 7 days of cessation of exposure, even though this model induced milder progenitor expansion and BM and blood eosinophilia than the other models (Figure 5F). In all 3 models, there was a noticeable correlation between the abundance of stage IV eosinophils in the BM and circulating blood eosinophils, which shared a similar $CCR3^+$ Siglec-F^+ phenotype (Figure 5B-F).

To identify the most prominent changes occurring in eosinophil lineage cells in response to eosinophilia-promoting stimuli, we compared the transcriptomes of stage I to IV eosinophils from IL-33-treated mice with steady-state counterparts. In a PCA, stage I-III progenitors of IL-33-treated mice were shifted leftward in PC1, which captured 67% of the variance (Figure 6A). Genes with negative loadings in PC1 were enriched in cell-cycle related genes, whereas genes with positive loadings were enriched in genes associated with myeloid cell function (Figure 6B). Two major patterns of transcriptomic changes were noticeable in eosinophilia (Figure 6C-E and Table S8); first, 2 clusters enriched in genes related to leukocyte responses and maturation, such as *Ccr3*, displayed delayed upregulation along eosinophilopoiesis. Second, another large cluster of genes containing eosinophil granule-, cell cycle- and translation-associated genes retained elevated expression in stage III progenitors of IL-33-treated mice. In addition, bulk SCENIC analysis identified 2 major clusters of regulons differing between steady-state and eosinophilia that were congruent with the above mRNA expression patterns (Figure 6F); one cluster comprising transcription factors associated with immune responses such as AP-1 and NF-κB, whose upregulation was delayed in eosinophilia, and another cluster

containing E2Fs and MYC that remained upregulated in stage III. SCENIC also identified a third cluster comprising GATA2 that was upregulated at all stages of maturation and a fourth cluster featuring IRF8 that was downregulated throughout eosinophilopoiesis in IL-33-treated mice. Gene expression of the aforementioned transcription factors followed the same pattern as their regulons (Figure S5B).

The above transcriptomic observations suggested eosinophil progenitors from IL-33-treated mice acquired a fully mature phenotype slower, while retaining cell cycling activity for longer. In vivo 5-ethynyl-2'-deoxyuridine (EdU) nucleotide incorporation assays using a short 1-hour pulse confirmed this assumption. Not only was the percentage of EdU^+ stage I-II progenitors increased in the BM of IL-33-treated mice (Figure 6G, Figure S5C), the percentage of EdU^+ stage III eosinophils also increased up to ~20%, compared to ~2% in steady-state mice. Eosinophil progenitors developing during IL-33-promoted eosinophilia hence displayed increased cell cycling activity and retained the ability to divide for longer. We obtained similar results in models of *N. brasiliensis* infection as well as in the milder model of exposure to *A. alternata* (Figure 6H-I). Altogether, the above findings support the notion that eosinophil progenitor expansion in eosinophilia was sustained by a dynamic increase in transit amplification relying on the slower acquisition of a fully mature phenotype and increased and prolonged proliferation capacity.

IRF8 is not intrinsically essential to eosinophil maturation and expansion

To illustrate the tractability of our data in clarifying the molecular determinants of eosinophil development and expansion, we investigated the yet uncertain role of IRF8 in eosinophilopoiesis (Figure S5D-I). The pattern of mRNA expression of IRF8 and its predicted activity in eosinophilia were inconsistent with an essential intrinsic role in eosinophil lineage development or expansion. Still, in the steady-state, the BM of IRF8-deficient mice was highly eosinopenic (Figure S5F), as described previously [38]. Nevertheless, all stages of maturation of eosinophils were present in IRF8-deficient mice and their relative abundance was comparable to that of wild-type counterparts. Furthermore, in response to IL-33, stage I-III eosinophil progenitors of IRF8-deficient mice expanded and incorporated EdU with a magnitude comparable to wild-type controls (Figure S5D-G, compare with Figure 6G). BM eosinopenia in IRF8-deficient mice was on the other hand accompanied by a general depression of GATA1 lineage cells up to the HSPC pool, reflecting the profound perturbations of hematopoiesis in these mice (Figure S5G-I). Hence, eosinopenia in IRF8-deficient mice was not primarily

caused by an intrinsic defect of the eosinophil lineage, but mainly by perturbations of HSPCs upstream of eosinophil lineage commitment.

Depletion of IL-5 impairs expansion of eosinophil progenitors in steady-state and eosinophilia

Several mechanisms have been proposed to explain the reduction in blood eosinophilia following neutralization of IL-5, ranging from reduced commitment and expansion to maturational arrest of eosinophil progenitors [45,46]. To help better characterize the activities of IL-5 *in vivo*, we generated IL-5Rα reporter (IL5RAporter) mice allowing straightforward identification of cells expressing *Il5ra*. IL5RAporter mice harbor an inactivating knock-in eGFP-T2A-Cre transgene in frame with the start codon of the native *Il5ra* locus (Figure 7A). The IL5RAporter allele labelled stages I to IV of the eosinophil lineage as well as a small subset of B cells (Figure 7B, Figure S6A), in line with previous studies that reported on IL5RA gene expression in eosinophils and in a subset of B cells [47,48]. IL5RAporter mice may also be used to induce Cre recombination in the eosinophil lineage of floxed mice (Figure 7B). Of note, neutrophils have been reported to display high surface staining with T21 and REA343 anti-IL-5Rα antibodies in mice [5,49] (Figure S6B). Yet, neutrophils did not express the IL5RAporter transgene (Figure S6C) and neutrophils of *Il5ra*-deficient IL5RAporter$^{KI/KI}$ mice stained similarly to neutrophils from wild-type control mice with these anti-CD125 clones (Figure S6B), indicating they cross-react with an unidentified neutrophil antigen. A third clone, DIH37, did not display this unspecific staining of neutrophils, but generated only mildly higher median fluorescence intensity in control compared to IL-5Rα-deficient eosinophils (Figure S6B). IL5RAporter mice were therefore superior to currently available alternatives in identifying cell types expressing IL-5Rα in mice.

We used IL5RAporter$^{KI/+}$ mice to identify the earliest IL-5Rα-expressing hematopoietic progenitors in the murine BM by conventional flow cytometry. Consistent with our scRNAseq analysis, the IL5RAporter allele became expressed after the divergence point of the basophil/mast cell and eosinophil lineages, only in cells committed to the eosinophil fate (Figure 7C-D, and Figure S6D). These results establish that IL-5 can only be expected to directly influence eosinophilopoiesis after lineage commitment in mice.

Finally, we assessed the impact of the depletion of IL-5 on eosinophilopoiesis in the steady-state and in eosinophilia. We first inspected the consequences of genetic deletion of IL-

5 using *Il5*$^{-/-}$ mice. All stages of eosinophil maturation were still present in *Il5*$^{-/-}$ mice (Figure 7E). The abundance of stage I progenitors in IL-5-deficient mice was comparable to that of reference control values (Figure 7F), but lineage expansion along stages II and III was reduced, resulting in reduced mature BM eosinophil abundance. In addition, stimulation by repeated administration of IL-33 for 7 days failed to expand stage I-III progenitors in *Il5*$^{-/-}$ mice (Figure 7F). We also assessed the consequences of depleting IL-5 on established eosinophilia using neutralizing monoclonal antibodies. Treatment with anti-IL5 antibodies of wild-type mice rendered eosinophilic by injections of IL-33 accelerated the contraction of stage I-III eosinophil progenitors toward steady-state reference values (Figure 7G). Anti-IL-5 treatment led to earlier upregulation of genes associated with mature myelocyte function alongside earlier downregulation of genes associated with cell cycling and translation (Figure 7H-I), consistent with a decrease in transit-amplification. Altogether, these data indicate that IL-5 was an essential promoter of the post-commitment expansion of eosinophil progenitors through transit amplification in both the steady-state and in response to eosinophilia-promoting signals, but was not required for their maturation.

Discussion

Eosinophils remain one of the least understood immune cells when it comes to their biological functions and development. Notably, the rapidly expanding clinical implementation of precision therapies targeting eosinophils directly or indirectly in EADs calls for a refined understanding of the ontogeny, expansion mechanisms and responses to treatment of eosinophils in preclinical models and human beings. The primary aim of this work was to provide easily transposable flow cytometric methods and immunophenotypic and transcriptomic resources for the translational study of eosinophilopoiesis.

Eosinophils are evolutionarily versatile cells [50] and attention has been devoted to highlighting differences between murine and human eosinophils [51]. We show that the ontogeny of eosinophils may be more conserved than previously estimated. One notable difference between murine and human eosinophilopoiesis regards the expression of IL-5Rα. Human basophils express IL-5Rα [52], whereas their murine counterparts do not. We show that this difference is wired in the development of these lineages in each species. Noticeably yet, IL-5Rα expression was still lower in human basophil/mast cell progenitors than in their eosinophil-committed counterparts. This could contribute to the fact that basophils are comparatively less reduced than eosinophils in patients treated with the anti-IL-5Rα depleting antibody benralizumab [53].

Resolving eosinophilopoiesis is important for a correct understanding of the functioning of the eosinophil lineage, and we identified several pervasive and often cumulative prior limitations in this regard. First, the use of different phenotyping strategies for the identification of the earliest identifiable eosinophil progenitors on the one hand and their progeny on the other hand precluded an integrated view of eosinophil lineage development and dynamics. Second, popular anti-murine IL-5Rα/CD125 antibodies used for identifying eosinophil progenitors are shown here to generate unspecific staining. This calls for a reinterpretation of murine studies based on these reagents due to the risk of contamination of eosinophil lineage cells by neutrophil lineage cells. Finally, assumptions were often made based on models in which neutrophils and eosinophils share developmental proximity within the highly heterogeneous "GMP" or "CMP" compartments. These hypotheses should also be reevaluated. For instance, it was previously proposed that IRF8 is important in the GMP or CMP to upregulate GATA1 and promote eosinophil maturation and fate divergence away from the neutrophil and monocyte lineages [18,54]. Rather, we show that IRF8 deficiency is damaging

to eosinophil development mainly because it negatively impacts on the HSPC progenitors of all GATA1-expressing lineages, which are on a trajectory distinct from that of monocytes and neutrophils. Our phenotyping strategies and transcriptomic data will hence be useful to reevaluate prior models of eosinophilopoiesis.

The resources provided herein can also be used to better understand the cellular dynamics of eosinophil lineage expansion in eosinophilia, or the response of the lineage to therapeutic interventions. We show that eosinophil progenitor expansion during eosinophilia involves enhanced transit amplification. Our transcriptomic and functional analyses of the regulation of eosinophil lineage expansion concur with a model in which IL-5 bioavailability determines the amplitude of eosinophil progenitor transit amplification as a major mechanism of regulation of eosinophil output from the BM in the steady-state or in eosinophilia. We did not observe cellular or transcriptional signs of maturational arrest in eosinophil progenitors following IL-5 depletion, which argues against the frequently purported requirement of IL-5 for eosinophil maturation. This is also in line with the observation that residual eosinophils in *Il5*-deficient mice and in asthmatic patients treated with anti-IL-5 mepolizumab do not show overt signs of perturbed development [55]. Hence, antibodies that neutralize IL-5 essentially reduce BM and blood eosinophilia by inhibiting eosinophil lineage expansion, without compromising eosinophil maturation.

It is proposed based on the study of erythropoiesis that transit amplification of committed progenitors in hematopoiesis is a balancing act between pro-proliferative gene expression programs that antagonize terminal maturation, and anti-proliferative programs promoting terminal maturation [56]. Transit amplification in erythropoiesis notably increases in response to glucocorticoids by acting on this balance [56]. Eosinophils, which like erythrocytes belong to the GATA1 myeloid lineages, display a similar tunability of their transit amplification, of which IL-5 bioavailability is an essential rheostat. There is evidence that similar processes of post-commitment transit amplification also control non-GATA1 lineage expansion, notably that of neutrophils in emergency granulopoiesis [57]. Another known mechanism for increasing neutrophil and monocyte output from the BM in inflammatory conditions is the promotion of the commitment of HSPCs toward non-GATA1 myeloid lineages [58–60]. It has been suggested that eosinophil, basophil and mast cell fates co-segregate in an early fate decision within the GATA1 arm of myelopoiesis [61], and that basophils and BM-derived mast cells share a common progenitor pool [33]. To our knowledge, to date, no physiological mechanism upstream of eosinophil lineage commitment has been uncovered *in vivo* that would regulate the commitment of HSPCs toward EBMs or the eosinophil lineage. We show herein that, at least

in mice, the receptor to IL-5 is only expressed in committed eosinophil progenitors, which precludes a role of IL-5 in the balance between the commitment toward the eosinophil versus the basophil and mast cell lineages.

Many open questions remain about the biology of eosinophils, which could be rooted in their development. For instance, could eosinophil progenitors be imprinted and could this later affect the activity of their mature progeny [62]? Eosinophils have also been shown to be phenotypically and functionally diverse in different organs, but the potential contribution of developmental processes to subsequent said diversity remains unexplored. We anticipate that the resources provided herein will help in answering these questions.

Limitations of the study

Limitations of the current study include the absence of analyses in human BM in eosinophilia-promoting conditions. Is eosinophil lineage expansion a sustained process or does it involve dynamic, time-resolved pulses of progenitor expansion, as observed in our murine models, in different EADs? Our study also focused mostly on events affecting the eosinophil lineage in the BM. Dynamic assessment of the entire eosinophil compartment from the BM to the blood to peripheral tissues in the steady-state and eosinophilia-promoting conditions would complement this work and allow mathematical modelling of the flux of eosinophils. Finally, because human EBM express IL-5Rα unlike their murine counterparts, the effect of IL-5 on eosinophil versus basophil or mast cell lineage commitment, as well as its role in the potential transit amplification of basophil and mast cell progenitors, remain to be assessed.

Acknowledgements

JJ was supported by a PhD fellowship and CJD and F. Baron are Senior Research Associates of the FRS-FNRS (Fonds de la Recherche Scientifique-Fonds National de la Recherche Scientifique, Belgium). This work was supported by the Fonds Wetenschappelijk Onderzoek – Vlaanderen (FWO) and the FRS-FNRS under EOS projects number 30565447 (U-HEAD) and number G0H1222N (BENEFICIARIES), by a research project grant (T.0052.18 REGEOS) and a research credit grant (35278176) of the FRS-FNRS, by the Léon Fredericq Foundation (Liege University), and by Liege University. The authors thank the flow cytometry platform, the mouse facility, and the genomics platform of the GIGA Research Institute of the University of Liege. We also thank N. Jacobs for critical reading of the manuscript and R. Fares, C. François and I. Sbai for excellent technical and secretarial assistance.

Author contributions

Conceptualization, C.J. Desmet and F. Bureau; Methodology, J. Jorssen, G. Van Hulst and C.J. Desmet; Investigation, J. Jorssen, G. Van Hulst, K. Mollers, J. Pujol, G. Petrellis, S. Schetters, A. Baptista; Formal analysis, J. Jorssen, G. Van Hulst and C.J. Desmet; Resources, J. Caers, F. Baron, B. Lambrecht, B.G. Dewals; Writing-original draft, J. Jorssen, G. Van Hulst, C.J. Desmet; Writing-review and editing, B.G. Dewals, S. Schetters, A. Baptista, B.N. Lambrecht and F. Bureau; Visualization, J. Jorssen, G. Van Hulst and C.J. Desmet; Supervision, C.J. Desmet; Project Administration, C.J. Desmet and F. Bureau; Funding Acquisition, C.J. Desmet and F. Bureau

Declaration of interests

The authors declare no competing interests.

Main figure title and legends

Figure 1. Single-cell RNA sequencing combined with high dimension flow cytometric screening resolves murine eosinophilopoiesis. A. Revised hematopoietic tree adapted from [15]. **B.** UMAP and lineage annotation, based on lineage marker genes in Table S1, of steady-state murine BM progenitors in droplet-based scRNAseq (result of one experiment on 3 pooled mice, insert: overlayed expression of *Gata1* defining GATA1 lineages). **C.** Overlayed expression of HSC and eosinophil marker genes in B. **D-E.** Slingshot trajectory inference in HSC-containing clusters (HSPC) and eosinophil and basophil/mast cell lineage clusters sub-selected from B (D), overlayed with pseudotime on basophil and eosinophil cell trajectories (E). **F.** Overlayed expression of eosinophil marker gene *Epx* and of basophil marker gene *Cd200r3* in E. **G.** Experimental outline of a flow cytometric screening focused on the murine eosinophil lineage (more detail in Figure S3A-B). **H.** UMAP of an Infinity Flow-integrated 142-marker staining of dump-negative $CD45^+$ murine BM cells with major lineages annotated based on cell surface markers in Figure S3C and Table S3 (result of one experiment on 15 pooled mice). **I.** Overlayed staining intensity of selected markers in indicated insert in H. **J.** Gating strategy of $CD55^+$ HSPCs and projection on UMAP in H. **K.** Gating strategy of the EBM progenitor pool and projection on UMAP in H. (Baso: basophil, c-FI: background-corrected fluorescence intensity, EBM: eosinophil/basophil/mast cell progenitors, Eo: eosinophil, Ery: erythroid, FI: fluorescence intensity, HSC: hematopoietic stem cell). See also Figure S3 and Tables S1 and S3.

Figure 2. Murine eosinophilopoiesis progresses along a continuum of immunophenotypes. **A.** Infinity Flow-derived UMAP of eosinophil lineage cells in murine BM displaying 4 main immunophenotypes used to partition their maturation continuum into 4 stages (I to IV) with pseudodensity overlayed (left) and heatmap of their relative expression of highly expressed markers (right, see Table S4 for signal intensity of all markers staining eosinophil-lineage cells, result of one experiment on 15 pooled mice). **B.** 9-color flow cytometric panel allowing the separation of murine eosinophil maturation into 4 (I-IV) immunophenotypic stages (Infinity Flow-inferred markers in green). **C.** UMAP of murine viable dump-negative ($Ly6G^-$ $B220^-$ $NK1.1^-$ $CD90.2^-$) $CD45^+$ BM cells stained with marker panel in B as pseudodensity plot (left) or with maturation stages I to IV overlayed (right). **D.** Gating strategy, downstream of gating strategy in Figure S3D, used for partitioning eosinophil maturation into stages I to IV. **E.** Light imaging photographs of stage I-IV eosinophils (scale bar: 15 μm). **F-G.** Bulk RNA sequencing

comparisons of stage I-IV BM eosinophils from 3 donors presented in a principal component analysis (F, upper, dashed lines connect samples from the same donor), as heatmaps of differentially expressed genes (DEG) between each stage (F, lower) and as major co-regulated modules (G and Table S5). **H.** Gene ontology (GO) enrichment analysis on co-expressed gene modules in G (FDR: false discovery rate). **I.** Comparison of normalized gene expression of selected genes in F (box-and-whisker diagrams with minimum and maximum values as boundaries, one-way ANOVA followed by TukeyHSD tests). See also Figure S3 and Tables S4 and S5.

Figure 3. High dimension flow cytometric screening resolves human eosinophil ontogeny **A.** Experimental outline of a flow cytometric screening focused on the human eosinophil lineage (more detail in Figure S4A-B). **B.** UMAP of an Infinity Flow-integrated 153-marker staining of viable lineage-negative $CD45^+$ human BM cells with major lineages annotated based on cell surface markers in Figure S4C and Table S3 (result of one experiment). **C.** Overlayed staining intensity of selected markers in B. **D.** Gating strategy of early eosinophil progenitors (EoP, red) and basophil/mast cell progenitors (BMP, blue), relative staining intensity with anti-CD125 and projection on UMAP in B. (HSC: hematopoietic stem cells, MPP: multipotent progenitors). See also Figure S4 and Table S3.

Figure 4. High dimension flow cytometric screening resolves human eosinophil maturation. A. Infinity Flow-derived UMAP of eosinophil lineage cells in human BM displaying 4 main immunophenotypes used to partition their maturation into 4 stages (I to IV) with pseudodensity overlayed (result of one experiment). **B.** Heatmap of the relative expression of highly expressed markers in maturation stage I-IV eosinophils (signal intensity of all markers staining eosinophil-lineage cells is in Table S6) and 10-color flow cytometric panel for the partition of the maturation continuum of human eosinophils into 4 stages. **C.** UMAP of human eosinophil lineage cells stained with marker panel in C as pseudodensity plot (left) or with maturation stages overlayed (right). **D.** Gating strategy for partitioning human eosinophil maturation into stages I to IV. **E.** Light imaging photographs of stage I-IV eosinophils (scale bar: 10 μm). **F-G.** Bulk RNA sequencing comparisons of stage I-IV BM eosinophils from 3 donors presented in a principal component analysis (F, upper, dashed lines connect samples from the same donor), as heatmaps of differentially expressed genes (DEG) between each stage (F, lower) and as major co-regulated modules (G and Table S7). **H.** Gene ontology (GO)

enrichment analysis on co-expressed gene modules in G (FDR: false discovery rate). **I.** Comparison of normalized gene expression of selected genes in F (box-and-whisker diagrams with minimum and maximum values as boundaries, one-way ANOVA followed by TukeyHSD tests). See also Tables S6 and S7

Figure 5. Eosinophil lineage progenitors expand in models of eosinophilic conditions. A. Experimental outline of the induction of eosinophilia in mice by repeated treatment with recombinant IL-33. **B.** Abundance of stage I-IV eosinophils in the BM of mice in A. **C.** Abundance of eosinophils in the blood of mice in A. **D.** UMAP of BM cells in A with pseudodensity overlayed. **E.** Experimental outline (up) of the analysis of the abundance of stages I-IV BM eosinophils (lower left) and of blood eosinophils (lower right) in mice infected with *Nippostrongylus brasiliensis*. **F.** Experimental outline (up) of the analysis of the abundance of stages I-IV BM eosinophils (lower left) and of blood eosinophils (lower right) in mice intranasally instilled with extracts of the mold *Alternaria alternata*. (Data pooled from 2 independent experiments each with n=3/group presented as mean ± SD and analyzed by one-way ANOVA on each eosinophil subpopulation followed by TukeyHSD tests. Ns: not significant, *p<0.05, **p<0.01, ***p<0.001, ****p<1.10^{-4}, IP: intraperitoneal).

Figure 6. Increased transit amplification sustains eosinophil lineage expansion. A. PCA of the transcriptomes of stage I-IV murine eosinophils from mice in the steady-state or made eosinophilic by the administration of IL-33 for 7 days as in Figure 5A (n=3/group, dashed lines connect stages in each donor). **B.** GO enrichment analysis on the genes with positive or negative loadings in PC1 in A. **C.** Bulk RNA sequencing comparison of stage I-IV eosinophils in A with major co-regulated modules (see Table S8) and selected genes. **D.** GO enrichment analysis on co-regulated gene modules in C. **E.** Comparison of normalized gene expression of selected genes in C. **F.** Row-scaled heatmap of bulk SCENIC analysis of samples in A (left) and comparison of selected regulon activity (right) **G-I.** Comparison of 5-ethynyl-2'-deoxyuridine (EdU) incorporation after a one-hour pulse in models of eosinophilia elicited by recombinant IL-33 (**G**), *N. brasiliensis* (Nb) infection (**H**) or intranasal instillation of *A. alternata* (Aa) (**I**) as in Figure 5. (Data pooled from 2 independent experiments each with n=3/group). (E-I: box-and-whisker diagrams with minimum and maximum values as boundaries, 2-way ANOVA followed by TukeyHSD tests. FDR: false discovery rate). See also Table S8.

Figure 7. IL-5 promotes transit amplification of committed eosinophil progenitors. A. Schematic of the targeting of the *Il5ra* locus for the generation of IL5-Rα reporter mice. **B.** Representative flow cytometric analysis of the expression of the eGFP reporter (upper) and TdTomato expression (lower) in stage I-IV eosinophils from the indicated transgenic mice with non-transgenic littermate as control. **C.** UMAP of HSPCs (marked by c-kit^{hi} expression) and eosinophil (marked by CCR3) and basophil (marked by CD200R3) lineages in murine dump^{-} CD45^{+} CD55^{+} BM cells (EBM: eosinophil/basophil/mast cell progenitors, result of one experiment on 3 pooled mice). **D.** Projection on the UMAP in C of gated eosinophil and basophil progenitors (red, gated as in Figure S6D) and of eosinophil-committed progenitors identified by expression of the eGFP IL5RAporter transgene within EBM (orange). **E-F.** UMAP and abundance of stage I-IV eosinophils in the BM of steady-state *Il5*$^{-/-}$ mice and *Il5*$^{-/-}$ mice stimulated for 7 days with IL-33 as in Figure 5 (box-and-whisker diagrams with minimum and maximum values as boundaries, data pooled from 2 independent experiments each with n=3/group and analyzed by separate 2-way ANOVA followed by TukeyHSD tests comparing stage I-IV cell abundance in control versus IL-33-stimulated *Il5*$^{-/-}$ mice on the one hand, and in control *Il5*$^{-/-}$ mice versus reference wild-type values on the other hand, reference wild-type values were from steady-state mice in Figure 5). **G.** Abundance of stage I-IV eosinophils in the BM of mice treated for 7 days with IL-33 as in Figure 5 and receiving either an isotype control or anti-IL5 neutralizing antibodies starting on the 6th day. For comparison, data is overlayed on data from Figure 5B (grey) (data pooled from 2 independent experiments each with n=3/group presented as mean ± SD and analyzed by one-way ANOVA followed TukeyHSD tests). **H-I.** Heatmap of co-regulated modules (H) and GO enrichment analysis and comparison of the expression (I) of the indicated genes (n=3/group, box-and-whisker diagrams with minimum and maximum values as boundaries, 2-way ANOVA followed by TukeyHSD tests). See also Figure S6.

STAR Methods

RESOURCE AVAILABILITY

Lead contact

Further information and requests for resources and reagents should be directed to and will be fulfilled by the lead contact, Christophe J Desmet (christophe.desmet@uliege.be).

Materials availability

IL-5Rα reporter (IL5RAporter) mice described in this study are available upon request from the Lead contact with a signed MTA.

Data and code availability

- Bulk and single-cell RNA-sequencing data is available from the Gene Expression Omnibus database at the National Centre for Biotechnology Information and is publicly available as of the date of publication. Accession numbers are listed in the key resources table.
- This study did not involve original code. Software and packages used are listed in the key resources table. Scripts of the presented bioinformatic analyses are available upon request from the Lead contact.
- Any additional information required to reanalyze the data reported in this paper is available from the lead contact upon request.

EXPERIMENTAL MODEL AND STUDY PARTICIPANT DETAILS

Mouse studies

C57BL/6J and *Il5*$^{-/-}$ (C57BL/6-Il5$^{tm1Kopf/J}$) mice were purchased from The Jackson Laboratory. *Irf8*$^{-/-}$ mice were described previously [63]. All mice were housed and bred under standard conditions in institutional specific pathogen-free facilities. Age- and sex-matched (female and male) groups of mice were used at 8–16 weeks of age and, when exposed to different treatments, were randomly assigned to experimental groups. Experimenters were not blinded. All animal experiments were approved by the animal ethics committee of the University of Liege and complied with the Animal Research: Reporting of In Vivo Experiments guidelines, the European Union directive 2010/63/EU and the Declaration of Helsinki for the use and care of animals.

Human participants

Five healthy donors undergoing total hip replacement were recruited in the study for bone marrow sample collection. One sample (54-year-old female) was used to set up a backbone panel and a second (62-year-old male) to run a flow cytometric screening. The 3 other samples (73-year-old female, 50-year-old male and 80-year-old female) were used to sort and perform RNA sequencing on stages of eosinophil maturation. The study was approved by the local ethics committee (IACUC, University of Liège) and written informed consent was obtained from all study participants. This research was undertaken in accordance with The Code of Ethics of the World Medical Association (Declaration of Helsinki) for experiments involving humans and followed the Recommendations for the Conduct, Reporting, Editing and Publication of Scholarly Work in Medical Journals of the International Committee of Medical Journal Editors.

METHOD DETAILS

Generation of IL-5Rα reporter mice

IL-5Rα reporter (IL5RAporter) mice were generated by PolyGene AG (Rümlang, Switzerland) using homologous gene targeting in C57BL/6 embryonic stem (ES) cells. The *Il5ra* gene is stretched roughly over 38 kb on mouse chromosome 6. The gene codes for 3 known primary transcripts, translated into two different peptides: the IL5RA protein (415 amino acid residues, coded by transcripts 201 and 202) and a 75-amino acid peptide (coded by transcript 203). We exchanged the first coding exon of all transcripts (corresponding to exon 4 in transcript 202) with the CDS of eGFP-T2A-Cre in a way that the original initiating ATG becomes the initiating ATG of the eGFP-T2A-Cre construct, which is supplemented with a SV40 poly(A) signal. An FRT-flanked neomycin selection cassette is inserted immediately downstream and a fragment of 2.2 kbp is deleted, eliminating the region of exon 5. This targeting strategy disrupts the *Il5ra* gene, leading to its knock-out. The targeting construct, K128.8a, was assembled by conventional cloning using homology arms straddling exons 4 and 5 of the *Il5ra* gene retrieved from BAC RP23-238B21, some synthesized elements, and selection and expression cassettes available at PolyGene. The flanking homology arms were short (2.6 /2.5 kbp) due to DNA elements that are refractory to cloning in bacteria, and the linearized vector yielded poor targeting frequency upon electroporation. Consequently, CRISPR targeting was used to enhance the frequency of homologous targeting. CRISPR guides were designed to induce cuts

as close as possible to homology arms, cutting the genome but not affecting the targeting vector or the recombined target. ES clones were generated via colipofection (Invitrogen Lipofectamin LTX) using 1µg of the guide plasmids and 1µg of the unmodified circular homology donor vector followed by selection with 0.8µg /ml puromycin and 200µg/ml G418. Out of 288 tested clones, six clones with correct integration at both homology sites were identified by PCR and injected into C57Bl/6Ng blastocysts. Five chimeric males obtained from the blastocyst injections were mated to Flp-deleter mice on C57Bl/6Ng background to assess transmission to the germ line, and cause elimination of the neo cassette via Flp/FRT excision. Chimeric males derived from 2 separate clones displayed germline transmission within their first litter. The heterozygous genotype was pathologically unsuspicious.

Human bone marrow preparation

Bone marrow aspirates were obtained from the femur of donors undergoing total hip replacement. Bone marrow was collected by aspiration before removal of the femoral head. A bone biopsy needle was inserted at the greater trochanter. The surgeon aspirated bone marrow using a heparinised 10 mL syringe and transferred it to heparin tubes.

10X single-cell RNA sequencing

Myeloid progenitors were sorted from the bone marrow of steady-state C57Bl/6 mice using a BD FACSAria III (BD Biosciences) cell sorter as described in Rosu et al.[64]. Siglec-F^+ bone marrow leukocytes were sorted using the same instrument from C57Bl/6 mice injected for 7 days with IL-33. Cells were resuspended in Ca and Mg free PBS containing 0.4mg/ml of UltraPure™ BSA (Thermofisher, AM2616). In total, 16,000 sorted cells were submitted to the 10X Genomics pipeline for encapsulation aiming for a recovery of ~10,000 sequenced single cells as described in the manufacturer's instructions. Sequencing libraries were prepared using Chromium Single Cell 3' Reagent Kit V3 (10X Genomics) as per manufacturer's instructions. CDNA quality and quantity were controlled using Agilent High Sensitivity DNA Kit (Agilent) on a 2100 Bioanalyser (Agilent). Sequencing was performed on an Illumina NovaSeq 6000 sequencer using the following read lengths: 28 bp for Read1, 8bp for sample index and 80bp for Read2. Reads were mapped to the GRCm38 reference genome using Cell Ranger (v3.0.2).

10X Flex single-cell RNA sequencing combined with CITE-Seq

Single-cell suspension of mouse bone marrow from steady state CB57BL/6 mice was first incubated with TruStain FcX™ PLUS (anti-mouse CD16/32) Antibody (BioLegend, 156603) for 10 mins at 4°C,washed with PBS 1% BSA, spun at 300g for 5 mins and then stained for Ly6G-FITC (BioLegend, 127606), CD90.2-FITC (BioLegend, 140204), NK1.1-FITC (eBioscience, 11-5941-85), CD45R-FITC (eBioscience, 11-0452-85), CD55-Biotin (R&D systems, BAF5376), CD45-AF700 (BioLegend, 103128) CD115-BV786 (BD Biosciences, 750888) along with the following TotalSeq-B antibodies: TotalSeq™-B0014 anti-mouse/human CD11b (BioLegend, 101273), TotalSeq™-B0130 anti-mouse Ly-6A/E (Sca-1) (BioLegend, 108149), TotalSeq™-B0114 anti-mouse F4/80 (BioLegend, 123155), TotalSeq™-B0012 anti-mouse CD117 (c-Kit) (BioLegend, 105849), TotalSeq™-B0203 anti-mouse CD150 (SLAM) (BioLegend, 115951), TotalSeq™-B0115 anti-mouse FcεRIα (BioLegend, 134341), TotalSeq™-B0808 anti-mouse CD193 (CCR3) (BioLegend, 144529), TotalSeq™ B0570 anti-mouse/rat CD29 (BioLegend, 102239), TotalSeq™-B0431 anti-mouse CD170 (Siglec-F) (BioLegend, 155517) for 30 minutes on ice. Cells were washed and stained with TotalSeq™-B0952 PE Streptavidin (BioLegend, 405287) for 30 minutes on ice and washed again. Next, cells were fixed for 1 hour at room temperature using the Chromium Next GEM Single Cell Fixed RNA Sample Preparation Kit (10X Genomics, 1000414) according to manufacturer's instructions and $CD45^{+}CD55^{+}dump^{-}$ $CD115^{-}$ cells were sorted using a BD FACSAria III (BD Biosciences) cell sorter and collected into PBS containing 1% ultrapure BSA (Fisher Scientific, 10743447) and 0.4Unit/µl Protector RNase Inhibitor (Merck, 3335399001). 800,000 sorted cells were subsequently submitted to probe hybridization using the Chromium Fixed RNA Kit, Mouse Transcriptome (10X Genomics, 1000495) according to manufacturer's instructions and 16000 probed cells were submitted to GEM generation, barcoding and construction of libraries were performed using the Chromium Next GEM Chip Q Single Cell Kit (10X Genomics, 1000422) and the Fixed RNA Feature Barcode Kit (10X Genomics, 1000419) following the CG00047 user guide. cDNA quality and quantity were controlled using Agilent High Sensitivity DNA Kit (Agilent) on a 2100 Bioanalyser (Agilent). Sequencing was performed on an Illumina NovaSeq 6000 and reads were mapped to the probe set and antibody barcode sequences using Cell Ranger (v3.0.2).

Single-cell RNA sequencing data processing and analysis

Raw feature matrices obtained from Cell Ranger (v3.0.2) were converted into a Seurat object and analysed using Seurat V4 (v4.3.0)[65] in R (v4.0.3). Genes contained in at least 3 cells and cells containing at more than 725 (Myeloid progenitors) or 200 (Siglec-F^{+} Leukocytes) but less

than 7000 RNA features and with a percentage of mitochondrial genes comprised between 1 and 10% (Myeloid progenitors) or below 20% (Siglec-F$^+$ Leukocytes) were selected for subsequent analysis. Clustering was performed using the Leiden algorithm (v0.4.3)[66]. Slingshot (v1.8.0)[67] was used for lineage trajectory inference and pseudotime calculation. Regulon activities were computed with SCENIC (v1.3.1) and AUCell(v1.21.2) [64] as in: http://htmlpreview.github.io/?https://github.com/aertslab/SCENIC/blob/master/inst/doc/SCENIC_Running.html.

For fixed single-cell RNA sequencing combined CITE-seq, data was also analysed using Seurat V4 following the WNN pipeline (https://satijalab.org/seurat/articles/weighted_nearest_neighbor_analysis) and cells with at least 10 RNA features and 30 RNA counts were selected for analysis. Cells with low RNA content but at least 500 counts of any protein feature were also integrated to the analysis. Erythroid , basophil and eosinophil clusters were subselected in order to rerun the analysis focusing only on these lineages.

Single-cell RNA sequencing data from magnetically enriched SiglecF$^+$ cells from the bone marrow of steady state IL-5 transgenic mice was downloaded from: https://www.ncbi.nlm.nih.gov/geo/query/acc.cgi?acc=GSE182001 [8]. Cells with at least 200 but no more than 6000 RNA features, at least 500 RNA counts and a percentage of mitochondrial genes between 0 and 10% were used for subsequent analysis with SeuratV4. The 20 first principal components were used to compute Nearest Neighbors and UMAP and a resolution of 0.5 was used for Louvain Clustering.

Mouse and human single-cell suspensions

Mouse blood was collected from the orbital sinus of terminally anesthetized mice and incubated with in-house prepared ammonium chloride lysis buffer (UltraPure distilled water (Invitrogen) supplemented with 150mM NH4Cl, 10mM KHCO, and 0.1mM EDTA) at room temperature for 5 minutes to lyse red blood cells. Cell suspension was passed through a 70µM cell strainer to remove cell clumps and washed twice prior to surface marker staining.

Mouse bone marrow was recovered from hind leg bones (pelvis, tibia, and femur). Bones were flushed with 10mL ice-cold PBS and passed through a 70µM cell strainer to remove cell clumps. Recovered single-cell suspensions were incubated with ammonium chloride lysis buffer for red blood cell lysis. Single-cell suspensions were washed twice with PBS prior to surface marker staining.

Human bone marrow aspirates were washed twice by diluting 1:50 in PBS. Red blood cells were depleted using EasySep™ RBC Depletion Reagent for a total of three cycles (Stemcell, 18170) following the manufacturer's instructions. The recovered single-cell suspensions were washed twice with PBS prior to surface marker staining.

High dimensional flow cytometric screening

Single-cell suspensions of mouse bone marrow from CB57BL/6 mice were first stained for Ly6G-FITC (BioLegend, 127606), CD90.2-FITC (BioLegend, 140204), NK1.1-FITC (eBioscience, 11-5941-85), CD45R-FITC (eBioscience, 11-0452-85) for 30 minutes on ice. Samples were immunomagnetically enriched for cells of interest using EasySep™ FITC positive selection kit II (Stemcell, 17682) as described in the manufacturer's instructions. The negative fractions were subsequently stained on ice for 30 minutes using a 13-color backbone panel with the following antibodies: SCA-1-BUV395 (BD Biosciences, 563990), CD11b-BUV737 (BD Biosciences, 621800), CD115-BV421 (BD Biosciences, 743638), CD55-biotin-streptavidin-BV510 (R&D, BAF5376, BD Biosciences, 563261), CXCR2-BV605 (BD Biosciences, 747814), Siglec-F-BV711 (BD Biosciences, 740764), CD16/32-BV786 (BD Biosciences, 740851), c-Kit-BB700 (BD Biosciences, 566414), CD200R3-PE-cy7 (eBioscience, 25-2001-82), CCR3-APC (BioLegend, 144512), CD45-Alexa fluor 700 (BD Biosciences, 560510), and FcεR1α-APC-eFluor780 (eBioscience, 47-5898-82) in 1X BD Horizon™ Brilliant stain buffer (BD Biosciences, 563794) for 30 minutes on ice (Figure S2A). Cells were washed twice and aliquoted into individual wells (3.10^5 cells/well) all containing a different PE-conjugated antibody (LEGENDScreen™, BioLegend, 700003) and incubated for 30 minutes on ice.

Single cell suspensions of human bone marrow were stained on ice for 30 minutes with a 12-color backbone panel containing the following antibodies: CD38-BUV395 (BD Biosciences, 563811), CD34-BUV737 (BD Biosciences, 748739), CD125-biotin-streptavidin-BV421 (Miltenyi, 130-110-543, BD Biosciences, 563259), FcεR1α-BV510 (BD Biosciences, 747786), CD11b-BV711 (BioLegend, 101242), CD45-BV786 (BD Biosciences, 563716), lineage-FITC (BioLegend, 348801), Siglec-8-BB700 (BD Biosciences, 747867), CD200R-PE-cy7 (BioLegend, 329312), CCR3-APC (Miltenyi, 130-116-507), c-Kit-APC-R700 (BD Biosciences, 565195), and CD66b-APC-cy7 (BD Biosciences, 305126) in 1X BD Horizon™ Brilliant stain buffer (BD Biosciences, 563794) for 30 minutes at room temperature (Figure S3A). Cells were washed twice and aliquoted into individual wells all containing a specific PE-

conjugated marker (LEGENDScreen™, BioLegend, 700007) and incubated for 30 minutes at room temperature.

All mouse and human samples were washed twice and the final cell pellet was resuspended in FACS buffer supplemented with 5nM BD Via-Probe™ Green (BD Biosciences, 565802). The 96-wells plates were acquired on a 5-laser BD LSRFortessa cell analyser (BD biosciences).

All data were pre-processed using FlowJo™ software (BD Biosciences, version 10.8, Supplementary Figures 2B & 3B). Each FCS file was assessed for quality control and single viable $CD45^+$ $dump^-$ cells were selected for further analysis. Only markers with expression higher than background on any of the events within the pool of target cells were provided to the Infinity Flow pipeline totalling 163 markers for the human analysis and 142 for the mouse (Figure S3B and S4B). The Infinity Flow pipeline was run as described in Becht et al.[41]. with 4.10^4 target cells as input for human data and 5.10^4 cells for mouse data. Output FCS files were concatenated into a single file for downstream analysis using FlowJo™ software.

Cell sorting of stages of eosinophil maturation from mouse and human bone marrow

Suspensions of mouse bone marrow cells from CB57BL/6 at steady state and following 7 daily IL-33 intraperitoneal injections were first stained with anti-Ly6G-FITC (BioLegend, 127606), CD90.2-FITC (BioLegend, 140204), NK1.1-FITC (eBioscience, 11-5941-85), CD45R-FITC (eBioscience, 11-0452-85) for 30 minutes on ice. Samples were immunomagnetically enriched for cells of interest using EasySep™ FITC positive selection kit II (Stemcell, 17682) as described in the manufacturer's instructions. The negative fractions were subsequently stained for CD29-pacblue (BioLegend, 102224), F4/80-BV510 (BioLegend, 123125), SiglecF-BV711(BD Biosciences,740764), CD55-biotin-streptavidin-BV786 (R&D, BAF5376, BD Biosciences, 563858), c-Kit-BB700 (BD Biosciences, 566414), Pir-A/B-PE (BioLegend, 144104) and CD200R3-PE-cy7 (BioLegend, 142212) in 1X BD Horizon™ Brilliant stain buffer (BD Biosciences, 563794) for 30 minutes on ice.

Human bone marrow single cell suspensions were first stained with Lineage-cocktail (BioLegend, 348801) for 30 minutes on ice. Samples were immunomagnetically enriched for cells of interest using EasySep™ FITC positive selection kit II (Stemcell, 17682) as described in the manufacturer's instructions. The negative fractions were next stained for CD84-BV421 (BD Biosciences, 566904), FcεR1α-BV510 (BD Biosciences, 747786), CD11b-BV711 (BioLegend, 101242), CD45-BV786 (BD Biosciences, 563204), Siglec-8-BB700 (BD Biosciences, 747867), CD38-PE (BioLegend, 356604), CD200R-PE-cy7 (BioLegend,

329312), CCR3-APC (Miltenyi, 130-123-300), and CD66b-APC-cy7 (BioLegend, 305126) in 1X BD Horizon™ Brilliant stain buffer (BD Biosciences, 563794) for 30 minutes at room temperature.

All mouse and human cells suspensions were washed twice and resuspended in PBS supplemented with 5nM BD Via-Probe™ Green (BD Biosciences, 565802). Mouse and human eosinophil stages were sorted directly into TRIzol (ThermoFisher, 15596026) or into FACS buffer for bright-field microscopy using a BD FACSAria III (BD Biosciences) cell sorter with a 100μm nozzle. Sort purity was at 95 per cent or higher and samples were stored at -80°C for downstream RNA applications or processed immediately for bright-field microscopy.

Bright-field microscopy

Sorted human- and mouse bone marrow cells were sedimented at 300xg for 5 minutes and resuspended in Freeflex Geloplasma 3% (Fresenius Kabi, RVG 20107), loaded into a cytofunnel and spun at 800rpm for 4 minutes on a 12 samples rotor in a Tharmac Cellspin I machine. Slides were left to dry 30 minutes and cells were stained using Hemacolor Rapid staining kit (Sigma-Aldrich, 1116610001). Bright-field cell images were taken at 1500x total magnification using an oil immersion objective.

RNA extraction

Human blood and mouse bone marrow eosinophils were sorted as described above directly into TRIzol (ThermoFisher). For every mL of TRIzol, 200μL of chloroform was added, and the samples were vigorously mixed and incubated for 2 minutes at room temperature. Samples were centrifuged at 10,000xg for 15 minutes at 4°C to separate the phases. The RNA-containing upper aqueous phase was transferred to a new microcentrifuge tube containing 475μL of isopropanol and 2μL of glycoblue (ThermoFisher, AM9515). Samples were centrifuged at 10,000xg for 15 minutes and supernatant was discarded. One volume of 75% ethanol was added to wash the RNA pellet and samples were centrifuged at 10,000xg for 1 minute and supernatant was discarded. RNA pellet was resuspended in 40μL of DNase/RNase-free water for a 15-minute DNase treatment (Zymo Research, E1010). DNase treatment was followed by column-based RNA purification with the RNA Clean & concentrator-5 kit (Zymo Research, R1016). Briefly, 100μL of RNA binding buffer was added to every 50μL sample and mixed thoroughly. One volume of 100% ethanol was added and the sample was transferred into a Zymo-Spin™ IC column in a collection tube. Columns were centrifuged at 10,000xg for

30 seconds and flow-through was discarded. The column was washed once with RNA prep buffer and twice with RNA wash buffer, following the manufacturer's instructions. RNA was eluted in 10μL of DNase/RNase-free water and stored at -80°C. Integrity and quantity of purified RNA were assessed using the RNA 6000 Pico kit (Agilent) for the presence of 18s and 28s rRNA peaks.

RNA sequencing & data processing

Full length cDNA was prepared from isolated RNA using SMART-Seq v4 Ultra Low Input RNA kit (Takara Bio, 634889) following the manufacturer's instructions, with 17 cycles of cDNA amplification. Final cDNA quality was assessed using Agilent High Sensitivity DNA kit (Agilent, 5067-4626). cDNA libraries were prepared for sequencing using Nextera XT DNA library preparation kit (Illumina, FC-131-1024) using the manufacturer's instructions and samples were sequenced on a NovaSeq™ 6000 sequencing system (Illumina).

Differential gene expression analyses

Sequenced reads were aligned to the mouse genome (UCSC mm10) or the human genome (HG19) with RNA-seq Alignment (v2.0.2) using STAR aligner (version 2.6.1a) on BaseSpace (https://basespace.illumina.com). Uniquely mapped reads were used to calculate gene expression. Differential gene expression was calculated using DESeq2 (v1.26.0) in R (v4.1.2) [68]. For analysis of differential gene expression along steady-state human and murine eosinophilopoiesis, we performed a paired likelihood ratio test (LRT) comparing the full model (gene count~donor+stage) with a reduced model (gene count~donor) on well-expressed expressed genes (baseMean>100). For comparison of eosinophil maturation stages in steady-state and IL33-stimulated mice, we used a likelihood ratio test (LRT) comparing the full model (gene count~stage*condition) with a reduced model (gene count~stage) on well-expressed expressed genes (baseMean>100). Genes with FDR<1.10^{-4} were considered as differentially expressed. Co-regulated gene modules were computed using the DEGPattern function of DEGreport (v1.30.3) with default settings and a cluster size >100 or >50 genes.

Gene set enrichment analyses

Enrichment of specified gene sets in GeneOntology biological process gene signatures was calculated using ShinyGO (v0.77, http://bioinformatics.sdstate.edu/go/) with default parameters. Regulon activities were computed with SCENIC (v1.3.1) and AUCell (v1.21.2).

Genes not represented by at least 1 UMI in each sample on average were discarded. The subsequent first quartile of lowly expressed genes was also filtered out. In bulk RNAseq analyses, only regulons with at least 0.3 activity score in any of the samples were considered for subsequent analysis.

Models of eosinophilia using IL-33, *Nippostrongylus brasiliensis*, and *Alternaria alternata*

For the IL-33 model, CB57BL/6 mice were injected intraperitoneally with 400ng of recombinant murine IL-33 in sterile PBS (Biolegend, 580506) daily for 7 days. Single cell bone marrow suspensions were harvested at steady state and at days 2, 4, 7, 9, and 12 (Figure 5A). Single cell bone marrow suspensions of *Il5*$^{-/-}$ mice were harvested at steady state and at day 7. CB57BL/6 mice also receiving anti-IL-5 treatment in addition to IL-33 were injected intraperitoneally with 400μg of anti-IL-5 (BioLegend, 504318) in sterile PBS at day 6, 7, and 8.

Nippostrongylus brasiliensis parasites were maintained in male Wistar rats as described previously [43,44]. L3 larvae were subsequently isolated from 9 to 16-day fecal cultures using a Baermann apparatus. CB57BL/6 mice were subcutaneously infected with 500xL3 larvae in sterile PBS. Single cell bone marrow suspensions were harvested at steady state and at days 5, 8, and 15 (Figure 5E).

In the *Alternaria alternata* model, we intranasally administered 200 μg of *Alternaria alternata* extract (Citeq biologics, 09.01.26) in sterile PBS daily for 22 days to CB57BL/6 mice. Single cell bone marrow suspensions were harvested at steady state and at days 4, 8, 15, 22, and 30 (Figure 5F).

All recovered single cell bone marrow suspensions were subsequently immunophenotyped using the following 9-color conventional flow cytometry panel: CD29-Pacific Blue (BioLegend, 102224), F4/80-BV510 (BioLegend, 123125), Siglec-F-BV711(BD Biosciences,740764), CD55-biotin-streptavidin-BV786 (R&D, BAF5376, BD Biosciences, 563858), Ly6G-FITC (BioLegend, 127606), CD90.2-FITC (BioLegend, 140204), NK1.1-FITC (eBioscience, 11-5941-85), CD45R-FITC (eBioscience, 11-0452-85), c-Kit-BB700 (BD Biosciences, 566414), Pir-A/B-PE (BioLegend, 144104) and CD200R3-PE-cy7 (BioLegend, 142212), and CCR3-APC (BioLegend, 144512) in 1X BD Horizon™ Brilliant stain buffer (BD Biosciences, 563794) for 30 minutes on ice. Stained samples were washed twice and resuspended in FACS buffer supplemented with 5nM BD Via-Probe™ Green (BD Biosciences, 565802). All samples were acquired on a 5-laser BD LSRFortessa cell analyser

(BD biosciences) and recorded data were analysed using FlowJo™ software (BD Biosciences, version 10.8). Instrument daily laser variations were corrected using BD FACSDiva™ CS&T research beads (BD Biosciences, 655050) and linked custom application settings system. Viable single cells were normalised across the different samples and eosinophil stages were quantified as cells per million bone marrow cells.

DNA replication assays

CB57BL/6 mice at steady-state and in models of eosinophilia were injected intraperitoneally with 1mg of EdU (5-ethynyl-2'-deoxyuridine) in PBS exactly 1 hour before sacrifice. Bone marrow cells were submitted to Click-iT™ EDU Alexa Fluor™ 647 Flow Cytometry Assay Kit (Thermofisher, C10424) following the manufacturer's instructions. Single cell bone marrow suspensions were stained with anti-CD29-pacblue (BioLegend, 102224), F4/80-BV510 (BioLegend, 123125), Siglec-F-BV711 (BD Biosciences,740764), CD55-biotin-streptavidin-BV786 (R&D, BAF5376, BD Biosciences, 563858), Ly6G-FITC (BioLegend, 127606), CD90.2-FITC (BioLegend, 140204), NK1.1-FITC (eBioscience, 11-5941-85), CD45R-FITC (eBioscience, 11-0452-85), c-Kit-BB700 (BD Biosciences, 566414), Pir-A/B-PE (BioLegend, 144104) and CD200R3- PE-cy7 (BioLegend, 142212) in 1X BD Horizon™ Brilliant stain buffer (BD Biosciences, 563794) for 30 minutes on ice. All stained suspensions were washed twice and acquired on a 5-laser BD LSRFortessa cell analyser (BD biosciences) and recorded data were analysed using FlowJo™ software (BD Biosciences, version 10.8).

Characterization of *Il5ra* expression in murine bone marrow progenitor cells

Bone marrow cells were harvested from IL5RAporter heterozygote (Il5RAporter$^{KI/+}$) and CB57BL/6 (*Il5ra*$^{+/+}$) mice. Cells were first stained for Ly6G-biotin (BioLegend, 127604), CD90.2-biotin (BioLegend, 140314), NK1.1-biotin (BioLegend, 108704), CD45R-biotin (BioLegend, 103204) for 30 minutes on ice. Samples were then immunomagnetically enriched for cells of interest using EasySep™ biotin positive selection kit II (Stemcell, 17683) as described in the manufacturer's instructions. The negative fractions were subsequently stained for anti-SCA1-BV421 (BD Biosciences, 553108), F4/80-BV510 (BioLegend, 123125), CD150-BV711 (BioLegend, 115941), c-Kit- BB700 (BD Biosciences, 566414), CD55-PE (BioLegend, 131804), CD200R3- PE-cy7 (BioLegend, 142212), CD45-Alexa Fluor 700 (BioLegend, 110724), CD16/32-APC-Cy-7 (BioLegend, 101328), CD11b-BUV737 (BD Biosciences, 612800), and streptavidin-BUV395 (BD Biosciences, 564176) in 1X BD Horizon™ Brilliant stain buffer (BD Biosciences, 563794) for 30 minutes on ice. Samples were

washed twice and acquired on a 5-laser BD LSRFortessa cell analyser (BD biosciences) and recorded data were analysed using FlowJo™ software (BD Biosciences, version 10.8).

Characterization of *Il5ra*-expressing bone marrow leukocytes

We built a 19-color antibody panel allowing the characterization of a wide variety of white blood cell lineages within the bone marrow. Bone marrow cells were harvested from Il5RAporter$^{KI/+}$ and *Il5ra*$^{+/+}$ mice and were stained with SiglecH-BV480 (BD Biosciences, 752585), CD125-BV421 (BD Biosciences, 565015), FcεR1α-Pacific Blue (Sony biotechnology, 1271570), CD138-BV605 (Sony biotechnology, 1312580), c-Kit-BV650 (Sony biotechnology, 1275625), CD64-BV711 (Sony biotechnology, 1296555), CD19-BV750 (Sony biotechnology, 1177805), CD14-BV785 (Sony biotechnology, 1216685), CD3-Spark Blue 574 (Sony biotechnology, 1101380), Ly6G-PerCP (Sony biotechnology, 1238270), Siglec-F-PE (BD Biosciences, 552126), F4/80-PE-Dazzle 594 (Sony biotechnology, 1215730), NK1.1-Pe-Cy5 (Sony biotechnology, 138620), CD200R3-Pe-Cy7 (BioLegend, 329312), CD8a-PE-Fire700 (Sony biotechnology, 1103960), CCR3-APC (BioLegend, 144512), CD4-APC-Fire480 (Sony biotechnology, 1102400), and CD45-Alexa Fluor™ 700 (BioLegend, 110724) on ice for 30 minutes. Cells were washed twice and acquired on a 5 laser ID7000™ spectral cell analyser (Sony biotechnology). All recorded data were analysed using FlowJo™ software (BD Biosciences, version 10.8).

Assessment of staining and specificity of anti-murine CD125 antibodies

Bone marrow cells were harvested from homozygote IL5RAporter (Il5RAporter$^{KI/KI}$, which are knock-out for *Il5ra*) and *Il5ra*$^{+/+}$ mice. Cell suspensions were stained with SiglecF-BV421 (BD Biosciences, 562681), Ly6G-PerCP-Cy5.5 (BioLegend, 127615), and CCR3-APC (BioLegend, 144512) on ice for 30 minutes. Samples were subsequently aliquoted and stained with one of the following PE-conjugated anti-CD125 clones: T21 (BD Biosciences, 558488), REA343 (Miltenyi, 130-125-513), or DIH37 (BioLegend, 153403). All samples were washed twice and acquired on a BD FACSAria III (BD Biosciences) cell sorter. CD125^{+}Ly6G^{+} and CD125^{+}Ly6G^{-} were sorted using a 100µm nozzle into FACS buffer for bright field microscopy and recorded data were analysed using FlowJo™ software (BD Biosciences, version 10.8).

Quantification and statistical analyses

All statistical analyses were performed in R (v4.1.2). All experiments followed a randomized design. Sample sizes were determined by power analysis. Respect of statistical tests

assumptions and model fit were evaluated using diagnostic plots. Raw data were transformed when needed for normalization and back-transformed for graphical presentation. Sample size, number of independent experiments and statistical tests applied to each dataset are indicated in figure legends. For clarity of presentation, only results of intergroup comparisons of interest are displayed in figures.

KEY RESOURCES TABLE

REAGENT or RESOURCE	SOURCE	IDENTIFIER
Antibodies		
BD Horizon™ BV421 Streptavidin	BD Biosciences	Cat# 563259, RRID:AB_2869475
BD Horizon™ BV510 Streptavidin	BD Biosciences	Cat# 563261
BD Horizon™ BV786 Streptavidin	BD Biosciences	Cat# 563858, RRID:AB_2869529
CD16/32 (clone 2.4G2)	BD Biosciences	Cat# 740851, RRID:AB_2740505
CD115 (clone T38-320)	BD Biosciences	Cat# 743638, RRID:AB_2741648
CD117 (clone 2B8)	BioLegend	Cat# 105849, RRID:AB_2813938
CD117 (clone 2B8)	BD Biosciences	Cat# 566414 (also 566415), RRID:AB_2744269
CD117 (clone YB5.B8)	BD Biosciences	Cat# 565195, RRID:AB_2716871
CD11b (clone M1/70)	BioLegend	Cat# 101242 (also 101241), RRID:AB_2563310
CD11b (clone M1/70)	BioLegend	Cat# 101273, RRID:AB_2819781
CD11b (clone M1/70)	BD Biosciences	Cat# 612800, RRID:AB_2870127
CD125 (clone REA705	Miltenyi Biotec	Cat# 130-110-543, RRID:AB_2654803
CD150 (clone TC15-12F12.2)	BioLegend	Cat# 115951, RRID:AB_2860628
CD170 (clone S17007L)	BioLegend	Cat# 155517, RRID:AB_2876514
CD170 (clone E50-2440)	BD Biosciences	Cat# 740764, RRID:AB_2740427
CD182 (clone V48-2310)	BD Biosciences	Cat# 747814, RRID:AB_2872278
CD193 (clone J073E5)	BioLegend	Cat# 144529, RRID:AB_2941427
CD193 (clone J073E5)	BioLegend	Cat# 144512 (also 144511), RRID:AB_2565738
CD193 (clone REA574)	Miltenyi Biotec	Cat# 130-116-507, RRID:AB_2727580
CD200R (clone OX-108)	BioLegend	Cat# 329312 (also 329311), RRID:AB_2783197
CD200R3 (clone Ba13)	eBioscience	Cat# 25-2001-82, RRID:AB_2848310
CD200R3 (clone Ba13	BioLegend	Cat# 142212 (also 142211), RRID:AB_2814046
CD29 (clone HMβ1-1)	BioLegend	Cat# 102224, RRID:AB_2128079
CD29 (clone HMβ1-1)	BioLegend	Cat# 102239, RRID:AB_2936675
CD34 (clone 8G12)	BD Biosciences	Cat# 748739, RRID:AB_2873143
CD38 (clone HB7)	BD Biosciences	Cat# 563811 (also 563812), RRID:AB_2744372
CD38 (clone HB7)	BioLegend	Cat# 356603 (also 356604), RRID:AB_2561899
CD45 (clone 30-F11)	BioLegend	Cat# 103128 (also 103127), RRID:AB_493715
CD45 (clone 30-F11)	BD Biosciences	Cat# 560510, RRID:AB_1645208
CD45(clone HI30)	BD Biosciences	Cat# 563204, RRID:AB_2738067
CD45(clone HI30)	BD Biosciences	Cat# 563716, RRID:AB_2716864
CD45R (clone RA3-6B2)	eBioscience	Cat# 11-0452-85, RRID:AB_465055
CD55 (clone DAF)	R&D systems	Cat# BAF5376, RRID:AB_2075978

CD66b (clone G10F5)	BioLegend	Cat# 305125 (also 305126), RRID:AB_2750183
CD84 (clone 2G7)	BD Biosciences	Cat# 566094, RRID:AB_2739498
CD90.2 (clone 53-2.1)	BioLegend	(BioLegend Cat# 140304 (also 140303), RRID:AB_10642812)
F4/80 (clone BM8)	BioLegend	Cat# 123135, RRID:AB_2562622
F4/80 (clone BM8)	BioLegend	Cat# 123155, RRID:AB_2819847
FcεRIα (clone AER-37)	BD Biosciences	Cat# 747786, RRID:AB_2872250
FcεRIα (clone MAR-1)	BioLegend	Cat# 134341, RRID:AB_2860676
FcεRIα (clone MAR-1)	eBioscience	Cat# 47-5898-82 (also 47-5898), RRID:AB_2573990
Human Lineage Cocktail	BioLegend	Cat# 348801, RRID:AB_10612570
Ly-6A/E (clone D7)	Biolegend	Cat# 108149, RRID:AB_2832369
Ly-6A/E (clone D7)	BD Biosciences	Cat# 563990, RRID:AB_2738527
Ly-6G (clone 1A8)	BioLegend	Cat# 127606; RRID:AB_1236488
NK1.1 (clone PK136)	eBioscience	Cat# 11-5941-85, RRID:AB_465319
PIR-A/B	BioLegend	Cat# 144104 (also 144103), RRID:AB_11204242
Siglec-8 (clone 837535)	BD Biosciences	Cat# 747867, RRID:AB_2872329
TotalSeq™-B0952 PE Streptavidin	BioLegend	Cat# 405287
TruStain FcX™ PLUS	BioLegend	Cat# 156604
Ultra-LEAF™ Purified anti-mouse/human IL-5	BioLegend	Cat# 504316 (also 504313, 504314, 504315, 504317, 504318), RRID:AB_2814414
Biological samples		
Human Bone marrow biopsies	Biothèque hospitalo-universitaire de Liège (BHUL)	23143, 29980, 30030, 30139, 30163
Chemicals, peptides, and recombinant proteins		
BD Via-Probe™ Green	BD Biosciences	Cat# 565802
Freeflex Geloplasma 3%	Fresenius Kabi	Cat# RVG20107
GlycoBlue™ Coprecipitant (15 mg/mL)	Invitrogen™	Cat# AM9515
Horizon™ Brilliant stain buffer	BD Biosciences	Cat# 563794
Protector RNase Inhibitor	Merck	Cat# 3335399001
Recombinant murine interleukin-33	BioLegend	Cat# 580506
TRIzol™ Reagent	Invitrogen™	Cat# 15596026
UltraPure™ BSA (50 mg/mL)	Invitrogen™	Cat# 10743447
Critical commercial assays		
Chromium Single Cell 3' Reagent Kit V3	10X Genomics	Cat# 1000076 Cat# 1000077 Cat# 1000078
Chromium Fixed RNA Kit, Mouse Transcriptome	10X Genomics	Cat# 1000495
Chromium Next GEM Chip Q Single Cell Kit	10X Genomics	Cat# 1000422
Chromium Next GEM Single Cell Fixed RNA Sample Preparation Kit	10X Genomics	Cat# 1000414
Click-iT™ EDU Alexa Fluor™ 647 Flow Cytometry Assay Kit	ThermoFisher	Cat# C10424
DNase I Set	Zymo Research	Cat# E1010
EasySep™ FITC positive selection kit II	StemCell Technologies	Cat# 17682

EasySep™ RBC Depletion Reagent	StemCell Technologies	Cat# 18170
Fixed RNA Feature Barcode Kit	10X Genomics	Cat# 1000419
Hemacolor® Rapid staining of blood smear	Sigma-Aldrich	Cat# 1116610001
High Sensitivity DNA kit	Agilent	Cat# 5067-4626
LEGENDScreen™ Human PE kit	BioLegend	Cat# 700007
LEGENDScreen™ Mouse PE kit	BioLegend	Cat# 700003
Nextera XT DNA library preparation kit	Illumina	Cat# FC-131-1024
RNA Clean & Concentrator-5	Zymo Research	Cat# R1016
SMART-Seq v4 Ultra Low Input RNA kit	Takara Bio	Cat# 634889
Deposited data		
Human bone marrow eosinophil stages transcriptomes at steady state	This paper	GEO: GSE249011
Mouse bone marrow eosinophil stages transcriptomes at steady state and during IL-33 induced eosinophilia	This paper	GEO: GSE249011
Mouse bone marrow eosinophil stages transcriptomes during IL-33 induced eosinophilia treated with anti-IL-5	This paper	GEO: GSE249011
Single cell transcriptomes of Lin^- $c\text{-}Kit^+$ $IL7Ra^-$ bone marrow cells	This paper	GEO: GSE249011
Single cell transcriptomes and CITE-seq data of $CD55^+$ bone marrow cells	This paper	GEO: GSE249011
Single cell transcriptomes of Siglec-F^+ bone marrow cells during IL-33 induced eosinophilia	This paper	GEO: GSE249011
Single cell transcriptomes of Siglec-F^+ bone marrow cells from IL-5 transgenic mice	Gurtner et al., 2023 [8]	GEO: GSE182001
Experimental models: Organisms/strains		
C57BL/6J	The Jackson Laboratory	RRID:IMSR_JAX:000664
C57BL/6-$Il5^{tm1Kopf/J}$	The Jackson Laboratory	RRID:IMSR_JAX:003175
$Irf8^{-/-}$	VIB-UGent Center for Inflammation Research [63]	N/A
IL-5Rα reporter mice	This paper	N/A
B6.Cg-$Gt(ROSA)26Sor^{tm14(CAG-tdTomato)Hze/J}$	The Jackson Laboratory	RRID:IMSR_JAX:007914
Rat-adapted *Nippostrongylus brasiliensis*	Rolot et al., 2018 [44]	N/A
Software and algorithms		
AUCell	Aibar et al., 2017 [64]	https://www.bioconductor.org/packages/release/bioc/html/AUCell.html
Cell Ranger	10X Genomics	https://www.10xgenomics.com/support/software/cell-ranger/latest
FlowJo™ software	BD Biosciences	https://www.bdbiosciences.com/en-be/products/software/flowjo-v10-software
Leiden algorithm	Traag et al., 2019 [66]	https://github.com/vtraag/leidenalg
R	The R foundation	https://www.r-project.org/
SCENIC	Aibar et al., 2017 [64]	https://github.com/aertslab/SCENIC?tab=readme-ov-file
Seurat V4	Satija Lab	https://satijalab.org/seurat/

Slingshot	Street et al., 2018 [67]	https://bioconductor.org/packages/release/bioc/html/slingshot.html
UMAP	Becht et al., 2018 [31]	https://umap-learn.readthedocs.io/en/latest/
DESeq2	Love et al., 2014 [68]	https://github.com/thelovelab/DESeq2
ShinyGO (v0.77)	Ge et al., 2020 [69]	http://bioinformatics.sdstate.edu/go/
Other		
Alternaria alternata extract	Citeq Biologics	Cat# 09.01.26
BD FACSDiva™ CS&T Research Beads	BD Biosciences	Cat# 655051

Excel Supplemental Tables title and legends

Table S1. Top 100 marker genes and attributed cell lineage of cell clusters identified through Seurat and Leiden clustering in a scRNAseq analysis on lineage-negative c-Kit+ IL7Ra- progenitors from murine bone marrow in Figure 1B

Table S2. Top100 marker genes discriminating each eosinophil subset identified in the bone marrow of mice using BD Rhapsody by Gurtner et al. [8] (upper) or 10X Chromium (lower) in Figure S2A-B, related to Figure 1

Table S4. Background-corrected median fluorescence intensity of staining of eosinophil lineage cells by the indicated PE-conjugated antibodies in a flow cytometric screening for eosinophil markers on murine bone marrow cells (related to Figure 2A)

Table S5. Genes differentially expressed along steady-state murine eosinophilopoiesis attributed to co-expression modules in order of presentation in Figure 2G

Table S6. Background-corrected median fluorescence intensity of staining of eosinophil lineage cells by the indicated PE-conjugated antibodies in a flow cytometric screening for eosinophil markers on human bone marrow cells (related to Figure 4A-B)

Table S7. Genes differentially expressed along steady-state human eosinophilopoiesis attributed to co-expression modules in order of presentation in Figure 4G

Table S8. Genes differentially expressed along eosinophilopoiesis in IL-33-treated mice versus control counterparts attributed to co-expression modules in order of presentation in Figure 6C

References

1. Klion, A.D., Ackerman, S.J., and Bochner, B.S. (2020). Contributions of Eosinophils to Human Health and Disease. Annual Review of Pathology: Mechanisms of Disease *15*, 179–209. 10.1146/annurev-pathmechdis-012419-032756.
2. Jacobsen, E.A., Jackson, D.J., Heffler, E., Mathur, S.K., Bredenoord, A.J., Pavord, I.D., Akuthota, P., Roufosse, F., and Rothenberg, M.E. (2021). Eosinophil Knockout Humans: Uncovering the Role of Eosinophils Through Eosinophil-Directed Biological Therapies. Annual Review of Immunology *39*, 1. 10.1146/annurev-immunol-093019-125918.
3. Mitre, E., and Klion, A.D. (2021). Eosinophils and helminth infection: protective or pathogenic? Seminars in Immunopathology *43*, 363–381. 10.1007/s00281-021-00870-z.
4. Ignacio, A., Shah, K., Bernier-Latmani, J., Köller, Y., Coakley, G., Moyat, M., Hamelin, R., Armand, F., Wong, N.C., Ramay, H., et al. (2022). Small intestinal resident eosinophils maintain gut homeostasis following microbial colonization. Immunity *55*, 1250–1267. 10.1016/j.immuni.2022.05.014.
5. Mesnil, C., Raulier, S., Paulissen, G., Xiao, X., Birrell, M.A., Pirottin, D., Janss, T., Starkl, P., Ramery, E., Henket, M., et al. (2016). Lung-resident eosinophils represent a distinct regulatory eosinophil subset. J Clin Invest *126*, 3279–3295. 10.1172/JCI85664.
6. Bohrer, A.C., Castro, E., Hu, Z., Queiroz, A.T.L., Tocheny, C.E., Assmann, M., Sakai, S., Nelson, C., Baker, P.J., Ma, H., et al. (2021). Eosinophils are part of the granulocyte response in tuberculosis and promote host resistance in mice. Journal of Experimental Medicine *218*. 10.1084/jem.20210469.
7. Poznanski, S.M., Mukherjee, M., Zhao, N., Huang, C., Radford, K., Ashkar, A.A., and Nair, P. (2021). Asthma exacerbations on benralizumab are largely non-eosinophilic. Allergy *76*, 375–379. https://doi.org/10.1111/all.14514.
8. Gurtner, A., Borrelli, C., Gonzalez-Perez, I., Bach, K., Acar, I.E., Núñez, N.G., Crepaz, D., Handler, K., Vu, V.P., Lafzi, A., et al. (2023). Active eosinophils regulate host defence and immune responses in colitis. Nature *615*, 151–157. 10.1038/s41586-022-05628-7.
9. Brigger, D., Riether, C., van Brummelen, R., Mosher, K.I., Shiu, A., Ding, Z., Zbären, N., Gasser, P., Guntern, P., Yousef, H., et al. (2020). Eosinophils regulate adipose tissue inflammation and sustain physical and immunological fitness in old age. Nature Metabolism *2*, 688–702. 10.1038/s42255-020-0228-3.
10. Grisaru-Tal, S., Rothenberg, Marc.E., and Munitz, A. (2022). Eosinophil–lymphocyte interactions in the tumor microenvironment and cancer immunotherapy. Nature Immunology *23*, 1309–1316. 10.1038/s41590-022-01291-2.
11. Iwasaki, H., Mizuno, S., Mayfield, R., Shigematsu, H., Arinobu, Y., Seed, B., Gurish, M.F., Takatsu, K., and Akashi, K. (2005). Identification of eosinophil lineage–committed progenitors in the murine bone marrow. J Exp Med *201*, 1891 LP – 1897.
12. Mori, Y., Iwasaki, H., Kohno, K., Yoshimoto, G., Kikushige, Y., Okeda, A., Uike, N., Niiro, H., Takenaka, K., Nagafuji, K., et al. (2009). Identification of the human eosinophil lineage-committed progenitor: revision of phenotypic definition of the human common myeloid progenitor. J Exp Med *206*, 183 LP – 193.
13. Tusi, B.K., Wolock, S.L., Weinreb, C., Hwang, Y., Hidalgo, D., Zilionis, R., Waisman, A., Huh, J.R., Klein, A.M., and Socolovsky, M. (2018). Population snapshots predict early haematopoietic and erythroid hierarchies. Nature *555*, 54.

14. Weinreb, C., Rodriguez-Fraticelli, A., Camargo, F.D., and Klein, A.M. (2020). Lineage tracing on transcriptional landscapes links state to fate during differentiation. Science, eaaw3381. 10.1126/science.aaw3381.
15. Jacobsen, S.E.W., and Nerlov, C. (2019). Haematopoiesis in the era of advanced single-cell technologies. Nat Cell Biol *21*, 2–8. 10.1038/s41556-018-0227-8.
16. Drissen, R., Buza-Vidas, N., Woll, P., Thongjuea, S., Gambardella, A., Giustacchini, A., Mancini, E., Zriwil, A., Lutteropp, M., Grover, A., et al. (2016). Distinct myeloid progenitor-differentiation pathways identified through single-cell RNA sequencing. Nat Immunol *17*, 666–676.
17. Drissen, R., Thongjuea, S., Theilgaard-Mönch, K., and Nerlov, C. (2019). Identification of two distinct pathways of human myelopoiesis. Sci Immunol *4*, eaau7148. 10.1126/sciimmunol.aau7148.
18. Mack, E.A., and Pear, W.S. (2020). Transcription factor and cytokine regulation of eosinophil lineage commitment. Curr Opin Hematol *27*.
19. Dougan, M., Dranoff, G., and Dougan, S.K. (2019). GM-CSF, IL-3, and IL-5 Family of Cytokines: Regulators of Inflammation. Immunity *50*, 796–811. 10.1016/j.immuni.2019.03.022.
20. Foster, P.S., Hogan, S.P., Ramsay, A.J., Matthaei, K.I., and Young, I.G. (1996). Interleukin 5 deficiency abolishes eosinophilia, airways hyperreactivity, and lung damage in a mouse asthma model. Journal of Experimental Medicine *183*, 195–201. 10.1084/jem.183.1.195.
21. Kopf, M., Brombacher, F., Hodgkin, P.D., Ramsay, A.J., Milbourne, E.A., Dai, W.J., Ovington, K.S., Behm, C.A., Köhler, G., Young, I.G., et al. (1996). IL-5-Deficient Mice Have a Developmental Defect in CD5+ B-1 Cells and Lack Eosinophilia but Have Normal Antibody and Cytotoxic T Cell Responses. Immunity *4*, 15–24. 10.1016/S1074-7613(00)80294-0.
22. Jarick, K.J., Topczewska, P.M., Jakob, M.O., Yano, H., Arifuzzaman, M., Gao, X., Boulekou, S., Stokic-Trtica, V., Leclère, P.S., Preußer, A., et al. (2022). Non-redundant functions of group 2 innate lymphoid cells. Nature *611*, 794–800. 10.1038/s41586-022-05395-5.
23. Roufosse, F. (2018). Targeting the Interleukin-5 Pathway for Treatment of Eosinophilic Conditions Other than Asthma. Preprint.
24. Pavord, I.D., Menzies-Gow, A., Buhl, R., Chanez, P., Dransfield, M., Lugogo, N., Keene, O.N., Bradford, E.S., and Yancey, S.W. (2020). Clinical Development of Mepolizumab for the Treatment of Severe Eosinophilic Asthma: On the Path to Personalized Medicine. J Allergy Clin Immunol Pract. https://doi.org/10.1016/j.jaip.2020.08.039.
25. Howell, I., Howell, A., and Pavord, I.D. (2023). Type 2 inflammation and biological therapies in asthma: Targeted medicine taking flight. Journal of Experimental Medicine *220*, e20221212. 10.1084/jem.20221212.
26. FitzGerald, J.M., Bleecker, E.R., Nair, P., Korn, S., Ohta, K., Lommatzsch, M., Ferguson, G.T., Busse, W.W., Barker, P., Sproule, S., et al. (2016). Benralizumab, an anti-interleukin-5 receptor α monoclonal antibody, as add-on treatment for patients with severe, uncontrolled, eosinophilic asthma (CALIMA): a randomised, double-blind, placebo-controlled phase 3 trial. Lancet *388*, 2128–2141. https://doi.org/10.1016/S0140-6736(16)31322-8.
27. Castro, M., Corren, J., Pavord, I.D., Maspero, J., Wenzel, S., Rabe, K.F., Busse, W.W., Ford, L., Sher, L., FitzGerald, J.M., et al. (2018). Dupilumab Efficacy and Safety in Moderate-to-Severe Uncontrolled Asthma. New Engl J Med *378*, 2486–2496. 10.1056/NEJMoa1804092.

28. Diver, S., Khalfaoui, L., Emson, C., Wenzel, S.E., Menzies-Gow, A., Wechsler, M.E., Johnston, J., Molfino, N., Parnes, J.R., Megally, A., et al. (2021). Effect of tezepelumab on airway inflammatory cells, remodelling, and hyperresponsiveness in patients with moderate-to-severe uncontrolled asthma (CASCADE): a double-blind, randomised, placebo-controlled, phase 2 trial. The Lancet Respiratory Medicine *9*, 1299–1312. 10.1016/S2213-2600(21)00226-5.
29. Wechsler, M.E., Ruddy, M.K., Pavord, I.D., Israel, E., Rabe, K.F., Ford, L.B., Maspero, J.F., Abdulai, R.M., Hu, C.-C., Martincova, R., et al. (2021). Efficacy and Safety of Itepekimab in Patients with Moderate-to-Severe Asthma. New England Journal of Medicine *385*, 1656–1668. 10.1056/NEJMoa2024257.
30. Laurenti, E., and Göttgens, B. (2018). From haematopoietic stem cells to complex differentiation landscapes. Nature *553*, 418.
31. Becht, E., McInnes, L., Healy, J., Dutertre, C.-A., Kwok, I.W.H., Ng, L.G., Ginhoux, F., and Newell, E.W. (2019). Dimensionality reduction for visualizing single-cell data using UMAP. Nature Biotechnology *37*, 38–44. 10.1038/nbt.4314.
32. Giladi, A., Paul, F., Herzog, Y., Lubling, Y., Weiner, A., Yofe, I., Jaitin, D., Cabezas-Wallscheid, N., Dress, R., Ginhoux, F., et al. (2018). Single-cell characterization of haematopoietic progenitors and their trajectories in homeostasis and perturbed haematopoiesis. Nature Cell Biology *20*, 836–846. 10.1038/s41556-018-0121-4.
33. Dahlin, J.S., Hamey, F.K., Pijuan-Sala, B., Shepherd, M., Lau, W.W.Y., Nestorowa, S., Weinreb, C., Wolock, S., Hannah, R., Diamanti, E., et al. (2018). A single-cell hematopoietic landscape resolves 8 lineage trajectories and defects in Kit mutant mice. Blood *131*, e1 LP-e11.
34. Aibar, S., González-Blas, C.B., Moerman, T., Huynh-Thu, V.A., Imrichova, H., Hulselmans, G., Rambow, F., Marine, J.-C., Geurts, P., Aerts, J., et al. (2017). SCENIC: single-cell regulatory network inference and clustering. Nature Methods *14*, 1083.
35. Bettigole, S.E., Lis, R., Adoro, S., Lee, A.-H., Spencer, L.A., Weller, P.F., and Glimcher, L.H. (2015). The transcription factor XBP1 is selectively required for eosinophil differentiation. Nat Immunol *16*, 829–837.
36. Bedi, R., Du, J., Sharma, A.K., Gomes, I., and Ackerman, S.J. (2009). Human C/EBP-ϵ activator and repressor isoforms differentially reprogram myeloid lineage commitment and differentiation. Blood *113*, 317–327. 10.1182/blood-2008-02-139741.
37. Mack, E.A., Stein, S.J., Rome, K.S., Xu, L., Wertheim, G.B., Melo, R.C.N., and Pear, W.S. (2019). Trib1 regulates eosinophil lineage commitment and identity by restraining the neutrophil program. Blood *133*, 2413–2426. 10.1182/blood.2018872218.
38. Milanovic, M., Terszowski, G., Struck, D., Liesenfeld, O., and Carstanjen, D. (2008). IFN Consensus Sequence Binding Protein (Icsbp) Is Critical for Eosinophil Development1. The Journal of Immunology *181*, 5045–5053. 10.4049/jimmunol.181.7.5045.
39. Wilkerson, E.M., Johansson, M.W., Hebert, A.S., Westphall, M.S., Mathur, S.K., Jarjour, N.N., Schwantes, E.A., Mosher, D.F., and Coon, J.J. (2016). The Peripheral Blood Eosinophil Proteome. Journal of Proteome Research *15*, 1524–1533. 10.1021/acs.jproteome.6b00006.
40. Kwok, I., Becht, E., Xia, Y., Ng, M., Teh, Y.C., Tan, L., Evrard, M., Li, J.L.Y., Tran, H.T.N., Tan, Y., et al. (2020). Combinatorial Single-Cell Analyses of Granulocyte-Monocyte Progenitor Heterogeneity Reveals an Early Uni-potent Neutrophil Progenitor. Immunity. 10.1016/j.immuni.2020.06.005.

41. Becht, E., Tolstrup, D., Dutertre, C.-A., Morawski, P.A., Campbell, D.J., Ginhoux, F., Newell, E.W., Gottardo, R., and Headley, M.B. (2023). High-throughput single-cell quantification of hundreds of proteins using conventional flow cytometry and machine learning. Science Advances *7*, eabg0505. 10.1126/sciadv.abg0505.
42. Kotas, M.E., Dion, J., Van Dyken, S., Ricardo-Gonzalez, R.R., Danel, C.J., Taillé, C., Mouthon, L., Locksley, R.M., and Terrier, B. (2021). A role for IL-33–activated ILC2s in eosinophilic vasculitis. JCI Insight *6*. 10.1172/jci.insight.143366.
43. Bouchery, T., Volpe, B., Shah, K., Lebon, L., Filbey, K., LeGros, G., and Harris, N. (2017). The Study of Host Immune Responses Elicited by the Model Murine Hookworms Nippostrongylus brasiliensis and Heligmosomoides polygyrus. Current Protocols in Mouse Biology *7*, 236–286. https://doi.org/10.1002/cpmo.34.
44. Rolot, M., Dougall, A.M., Chetty, A., Javaux, J., Chen, T., Xiao, X., Machiels, B., Selkirk, M.E., Maizels, R.M., Hokke, C., et al. (2018). Helminth-induced IL-4 expands bystander memory CD8+ T cells for early control of viral infection. Nature Communications *9*, 4516. 10.1038/s41467-018-06978-5.
45. Fulkerson, P.C., Schollaert, K.L., Bouffi, C., and Rothenberg, M.E. (2014). IL-5 Triggers a Cooperative Cytokine Network That Promotes Eosinophil Precursor Maturation. J Immunol *193*, 4043 LP – 4052. 10.4049/jimmunol.1400732.
46. Menzies-Gow, A., Flood-Page, P., Sehmi, R., Burman, J., Hamid, Q., Robinson, D.S., Kay, A.B., and Denburg, J. (2003). Anti-IL-5 (mepolizumab) therapy induces bone marrow eosinophil maturational arrest and decreases eosinophil progenitors in the bronchial mucosa of atopic asthmatics. J Allergy Clin Immunol *111*, 714–719. 10.1067/mai.2003.1382.
47. Yoshida, T., Ikuta, K., Sugaya, H., Maki, K., Takagi, M., Kanazawa, H., Sunaga, S., Kinashi, T., Yoshimura, K., Miyazaki, J., et al. (1996). Defective B-1 Cell Development and Impaired Immunity against Angiostrongylus cantonensis in IL-5Rα-Deficient Mice. Immunity *4*, 483–494. 10.1016/S1074-7613(00)80414-8.
48. Wang, W., Xu, Y., Wang, L., Zhu, Z., Aodeng, S., Chen, H., Cai, M., Huang, Z., Han, J., Wang, L., et al. (2022). Single-cell profiling identifies mechanisms of inflammatory heterogeneity in chronic rhinosinusitis. Nature Immunology *23*, 1484–1494. 10.1038/s41590-022-01312-0.
49. Grisaru-Tal, S., Dulberg, S., Beck, L., Zhang, C., Itan, M., Hediyeh-zadeh, S., Caldwell, J., Rozenberg, P., Dolitzky, A., Avlas, S., et al. (2021). Metastasis-Entrained Eosinophils Enhance Lymphocyte-Mediated Antitumor Immunity. Cancer Research *81*, 5555–5571. 10.1158/0008-5472.CAN-21-0839.
50. Stacy, N.I., and Ackerman, S.J. (2021). A tribute to eosinophils from a comparative and evolutionary perspective. J Allergy Clin Immunol. 10.1016/j.jaci.2020.12.002.
51. Lee, J.J., Jacobsen, E.A., Ochkur, S.I., McGarry, M.P., Condjella, R.M., Doyle, A.D., Luo, H., Zellner, K.R., Protheroe, C.A., Willetts, L., et al. (2012). Human versus mouse eosinophils: "that which we call an eosinophil, by any other name would stain as red." J Allergy Clin Immunol *130*, 572–584. 10.1016/j.jaci.2012.07.025.
52. Wright, A.K.A., Weston, C., Rana, B.M.J., Brightling, C.E., and Cousins, D.J. (2017). Human group 2 innate lymphoid cells do not express the IL-5 receptor. Journal of Allergy and Clinical Immunology *140*, 1430-1433.e4. https://doi.org/10.1016/j.jaci.2017.04.025.
53. Lommatzsch, M., Marchewski, H., Schwefel, G., Stoll, P., Virchow, J.C., and Bratke, K. (2020). Benralizumab strongly reduces blood basophils in severe eosinophilic asthma. Clinical & Experimental Allergy *50*, 1267–1269. https://doi.org/10.1111/cea.13720.

54. Willebrand, R., and Voehringer, D. (2017). Regulation of eosinophil development and survival. Current Opinion in Hematology *24*.
55. Van Hulst, G., Jorssen, J., Jacobs, N., Henket, M., Louis, R., Schleich, F., Bureau, F., and Desmet, C.J. (2022). Anti-IL-5 mepolizumab minimally influences residual blood eosinophils in severe asthma. European Respiratory Journal *59*, 2100935. 10.1183/13993003.00935-2021.
56. Li, H., Natarajan, A., Ezike, J., Barrasa, M.I., Le, Y., Feder, Z.A., Yang, H., Ma, C., Markoulaki, S., and Lodish, H.F. (2019). Rate of Progression through a Continuum of Transit-Amplifying Progenitor Cell States Regulates Blood Cell Production. Dev Cell *49*, 118-129.e7. https://doi.org/10.1016/j.devcel.2019.01.026.
57. Hérault, A., Binnewies, M., Leong, S., Calero-Nieto, F.J., Zhang, S.Y., Kang, Y.-A., Wang, X., Pietras, E.M., Chu, S.H., Barry-Holson, K., et al. (2017). Myeloid progenitor cluster formation drives emergency and leukaemic myelopoiesis. Nature *544*, 53–58. 10.1038/nature21693.
58. Mossadegh-Keller, N., Sarrazin, S., Kandalla, P.K., Espinosa, L., Stanley, E.R., Nutt, S.L., Moore, J., and Sieweke, M.H. (2013). M-CSF instructs myeloid lineage fate in single haematopoietic stem cells. Nature *497*, 239–243. 10.1038/nature12026.
59. Schultze, J.L., Mass, E., and Schlitzer, A. (2019). Emerging Principles in Myelopoiesis at Homeostasis and during Infection and Inflammation. Immunity *50*, 288–301. 10.1016/j.immuni.2019.01.019.
60. Hysenaj, L., de Laval, B., Arce-Gorvel, V., Bosilkovski, M., González-Espinoza, G., Debroas, G., Sieweke, M.H., Sarrazin, S., and Gorvel, J.-P. (2023). CD150-dependent hematopoietic stem cell sensing of Brucella instructs myeloid commitment. Journal of Experimental Medicine *220*, e20210567. 10.1084/jem.20210567.
61. Wang, S.-W., Herriges, M.J., Hurley, K., Kotton, D.N., and Klein, A.M. (2022). CoSpar identifies early cell fate biases from single-cell transcriptomic and lineage information. Nature Biotechnology. 10.1038/s41587-022-01209-1.
62. Van Hulst, G., Bureau, F., and Desmet, C.J. (2021). Eosinophils as Drivers of Severe Eosinophilic Asthma: Endotypes or Plasticity? Preprint, 10.3390/ijms221810150 10.3390/ijms221810150.
63. Sichien, D., Scott, C.L., Martens, L., Vanderkerken, M., Van Gassen, S., Plantinga, M., Joeris, T., De Prijck, S., Vanhoutte, L., Vanheerswynghels, M., et al. (2016). IRF8 Transcription Factor Controls Survival and Function of Terminally Differentiated Conventional and Plasmacytoid Dendritic Cells, Respectively. Immunity *45*, 626–640. https://doi.org/10.1016/j.immuni.2016.08.013.
64. Rosu, A., El Hachem, N., Rapino, F., Rouault-Pierre, K., Jorssen, J., Somja, J., Ramery, E., Thiry, M., Nguyen, L., Jacquemyn, M., et al. (2021). Loss of tRNA-modifying enzyme Elp3 activates a p53-dependent antitumor checkpoint in hematopoiesis. Journal of Experimental Medicine *218*, e20200662. 10.1084/jem.20200662.
65. Hao, Y., Hao, S., Andersen-Nissen, E., Mauck III, W.M., Zheng, S., Butler, A., Lee, M.J., Wilk, A.J., Darby, C., Zager, M., et al. (2021). Integrated analysis of multimodal single-cell data. Cell *184*, 3573-3578.e29. 10.1016/j.cell.2021.04.048.
66. Traag, V.A., Waltman, L., and van Eck, N.J. (2019). From Louvain to Leiden: guaranteeing well-connected communities. Scientific Reports *9*, 5233. 10.1038/s41598-019-41695-z.
67. Street, K., Risso, D., Fletcher, R.B., Das, D., Ngai, J., Yosef, N., Purdom, E., and Dudoit, S. (2018). Slingshot: cell lineage and pseudotime inference for single-cell transcriptomics. BMC Genomics *19*, 477. 10.1186/s12864-018-4772-0.

68. Love, M.I., Huber, W., and Anders, S. (2014). Moderated estimation of fold change and dispersion for RNA-seq data with DESeq2. Genome Biol *15*, 550. 10.1186/s13059-014-0550-8.
69. Ge, S.X., Jung, D., and Yao, R. (2020). ShinyGO: a graphical gene-set enrichment tool for animals and plants. Bioinformatics 36, 2628. 10.1093/bioinformatics/btz931.

Figure 1

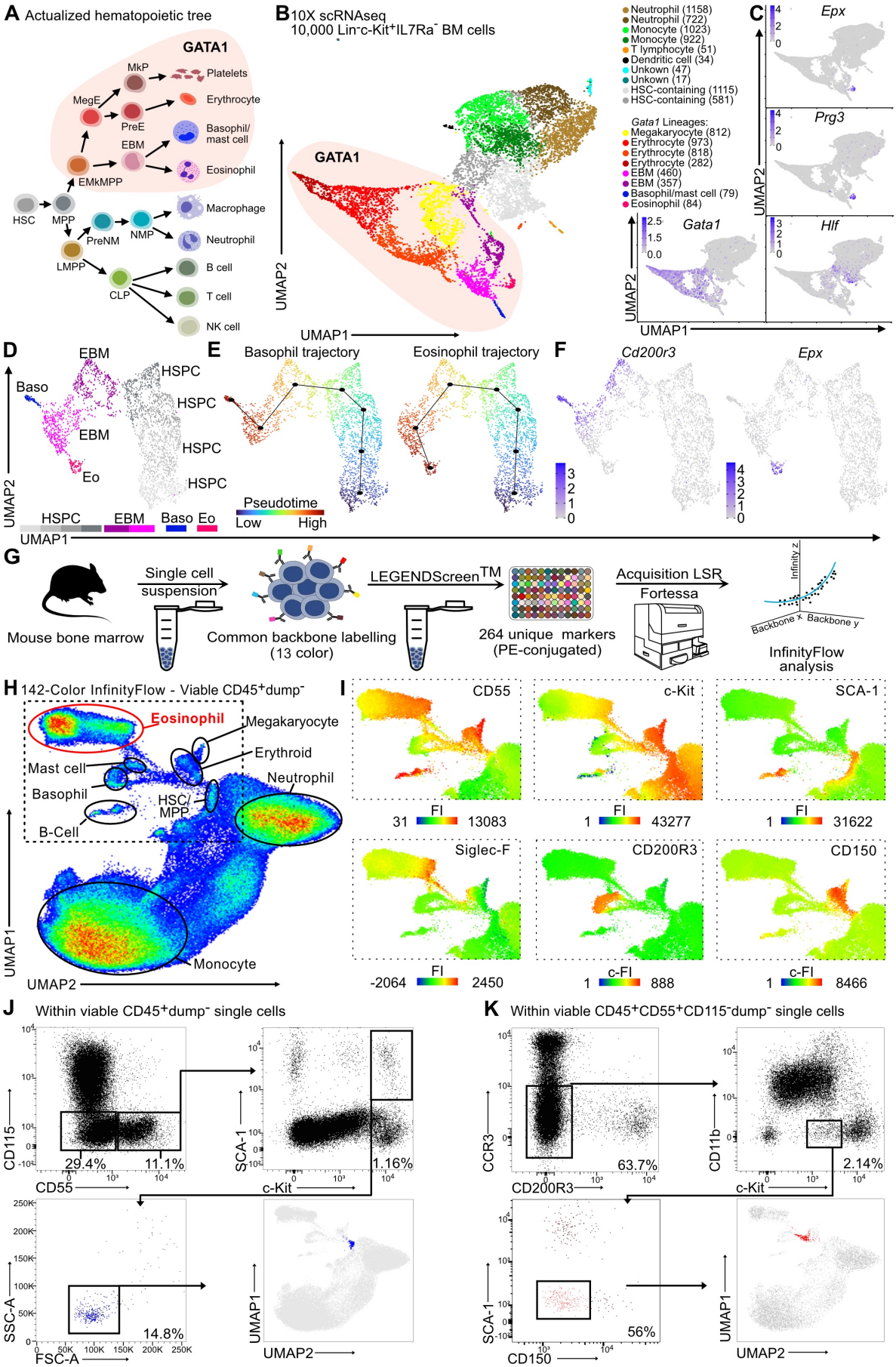
A Actualized hematopoietic tree
GATA1
MkP
Platelets
MegE
Erythrocyte
PreE
Basophil/ mast cell
EBM
Eosinophil
EMkMPP
HSC
MPP
Macrophage
PreNM
NMP
Neutrophil
LMPP
B cell
CLP
T cell
NK cell
B 10X scRNAseq
10,000 Lin-c-Kit+IL7Ra- BM cells
GATA1
UMAP2
UMAP1
Neutrophil (1158)
Neutrophil (722)
Monocyte (1023)
Monocyte (922)
T lymphocyte (51)
Dendritic cell (34)
Unkown (47)
Unkown (17)
HSC-containing (1115)
HSC-containing (581)
Gata1 Lineages:
Megakaryocyte (812)
Erythrocyte (973)
Erythrocyte (818)
Erythrocyte (282)
EBM (460)
EBM (357)
Basophil/mast cell (79)
Eosinophil (84)
C
Epx
Prg3
Gata1
Hlf
UMAP2
UMAP1
D
EBM
Baso
HSPC
HSPC
EBM
HSPC
Eo
HSPC
UMAP2
HSPC EBM Baso Eo
UMAP1
E
Basophil trajectory
Eosinophil trajectory
Pseudotime
Low High
F
Cd200r3
Epx
G
Mouse bone marrow
Single cell suspension
Common backbone labelling (13 color)
LEGENDScreen™
264 unique markers (PE-conjugated)
Acquisition LSR Fortessa
Infinity z
Backbone x
Backbone y
InfinityFlow analysis
H 142-Color InfinityFlow - Viable CD45+dump-
Eosinophil
Megakaryocyte
Erythroid
Mast cell
Neutrophil
Basophil
HSC/ MPP
B-Cell
Monocyte
UMAP1
UMAP2
I
CD55
c-Kit
SCA-1
31 FI 13083
1 FI 43277
1 FI 31622
Siglec-F
CD200R3
CD150
-2064 FI 2450
1 c-FI 888
1 c-FI 8466
J Within viable CD45+dump- single cells
CD115
CD55
29.4%
11.1%
SCA-1
c-Kit
1.16%
SSC-A
FSC-A
14.8%
UMAP1
UMAP2
K Within viable CD45+CD55+CD115-dump- single cells
CCR3
CD200R3
63.7%
CD11b
c-Kit
2.14%
SCA-1
CD150
56%
UMAP1
UMAP2

Figure 2

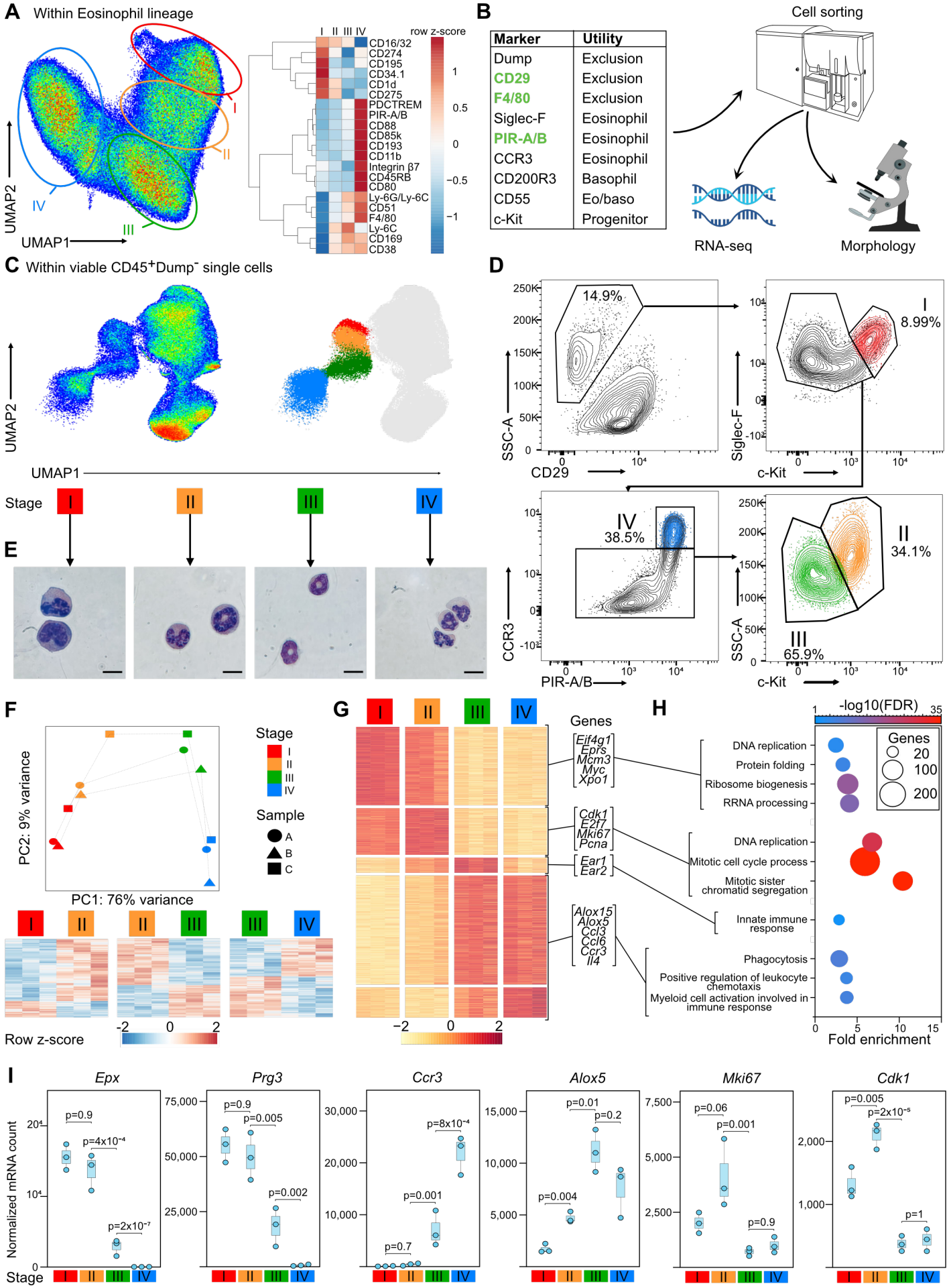
A
Within Eosinophil lineage
UMAP2
UMAP1
I
II
III
IV
I II III IV
row z-score
CD16/32
CD274
CD195
CD34.1
CD1d
CD275
PDCTREM
PIR-A/B
CD88
CD85k
CD193
CD11b
Integrin β7
CD45RB
CD80
Ly-6G/Ly-6C
CD51
F4/80
Ly-6C
CD169
CD38
1
0.5
0
−0.5
−1
B
Marker
Utility
Dump
Exclusion
CD29
Exclusion
F4/80
Exclusion
Siglec-F
Eosinophil
PIR-A/B
Eosinophil
CCR3
Eosinophil
CD200R3
Basophil
CD55
Eo/baso
c-Kit
Progenitor
Cell sorting
RNA-seq
Morphology
C
Within viable CD45+Dump- single cells
UMAP2
UMAP1
Stage
I
II
III
IV
D
14.9%
SSC-A
CD29
I
8.99%
Siglec-F
c-Kit
IV
38.5%
CCR3
PIR-A/B
II
34.1%
III
65.9%
SSC-A
c-Kit
E
F
PC2: 9% variance
PC1: 76% variance
Stage
Sample
A
B
C
Row z-score
G
Genes
Eif4g1
Eprs
Mcm3
Myc
Xpo1
Cdk1
E2f7
Mki67
Pcna
Ear1
Ear2
Alox15
Alox5
Ccl3
Ccl6
Ccr3
Il4
H
-log10(FDR)
Genes
20
100
200
DNA replication
Protein folding
Ribosome biogenesis
RRNA processing
DNA replication
Mitotic cell cycle process
Mitotic sister chromatid segregation
Innate immune response
Phagocytosis
Positive regulation of leukocyte chemotaxis
Myeloid cell activation involved in immune response
Fold enrichment
I
Epx
Prg3
Ccr3
Alox5
Mki67
Cdk1
Normalized mRNA count
Stage
p=0.9
p=4x10-4
p=2x10-7
p=0.9
p=0.005
p=0.002
p=0.7
p=0.001
p=8x10-4
p=0.004
p=0.01
p=0.2
p=0.06
p=0.001
p=0.9
p=0.005
p=2x10-5
p=1

Figure 3

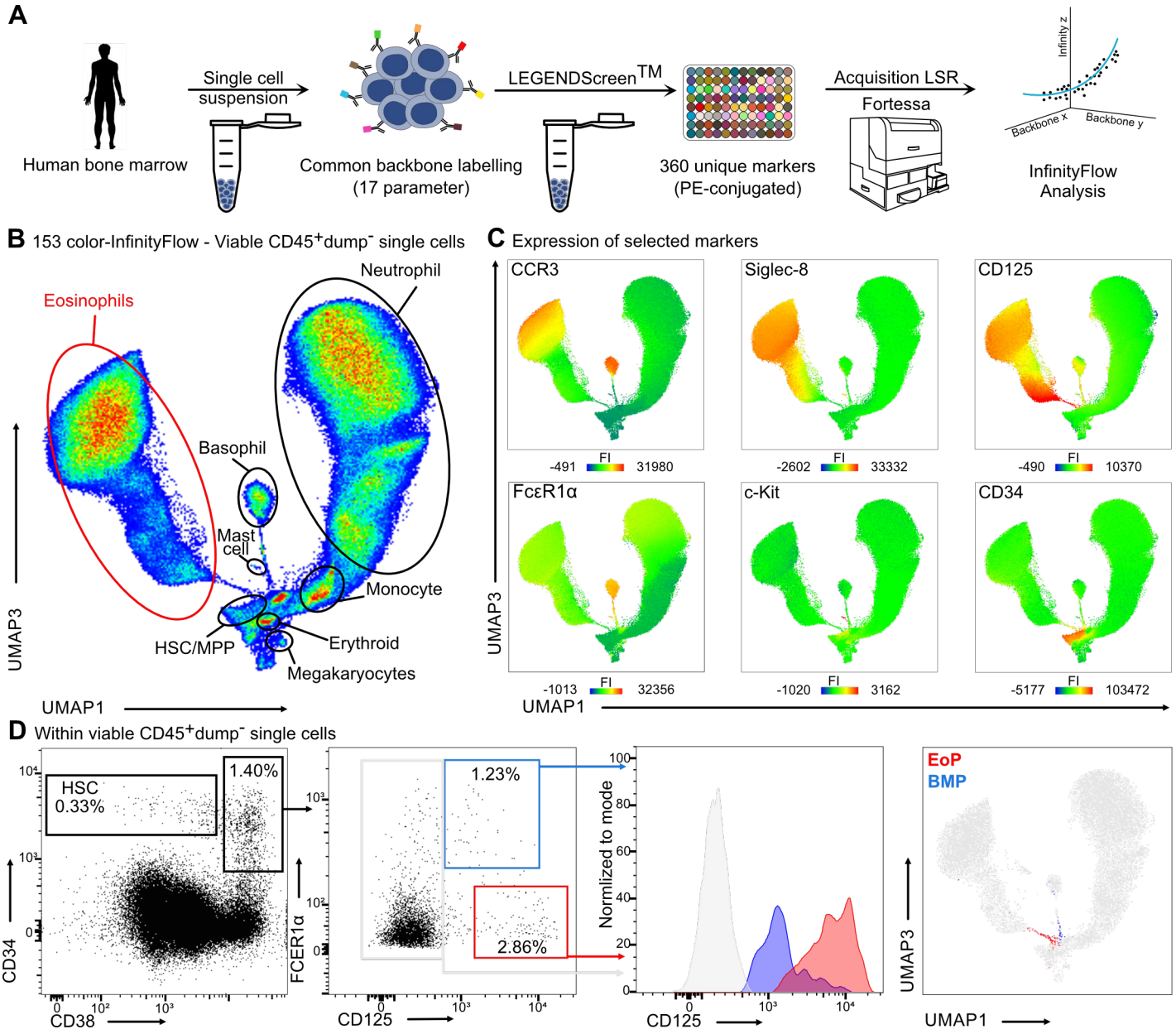
A
Human bone marrow
Single cell suspension
Common backbone labelling (17 parameter)
LEGENDScreen™
360 unique markers (PE-conjugated)
Acquisition LSR Fortessa
InfinityFlow Analysis
Infinity z
Backbone x
Backbone y
B 153 color-InfinityFlow - Viable CD45+dump- single cells
Eosinophils
Neutrophil
Basophil
Mast cell
Monocyte
HSC/MPP
Erythroid
Megakaryocytes
UMAP3
UMAP1
C Expression of selected markers
CCR3
Siglec-8
CD125
FcεR1α
c-Kit
CD34
FI
-491
31980
-2602
33332
-490
10370
-1013
32356
-1020
3162
-5177
103472
UMAP3
UMAP1
D Within viable CD45+dump- single cells
HSC
0.33%
1.40%
CD34
CD38
FCER1α
CD125
1.23%
2.86%
Normlized to mode
CD125
EoP
BMP
UMAP3
UMAP1

Figure 4

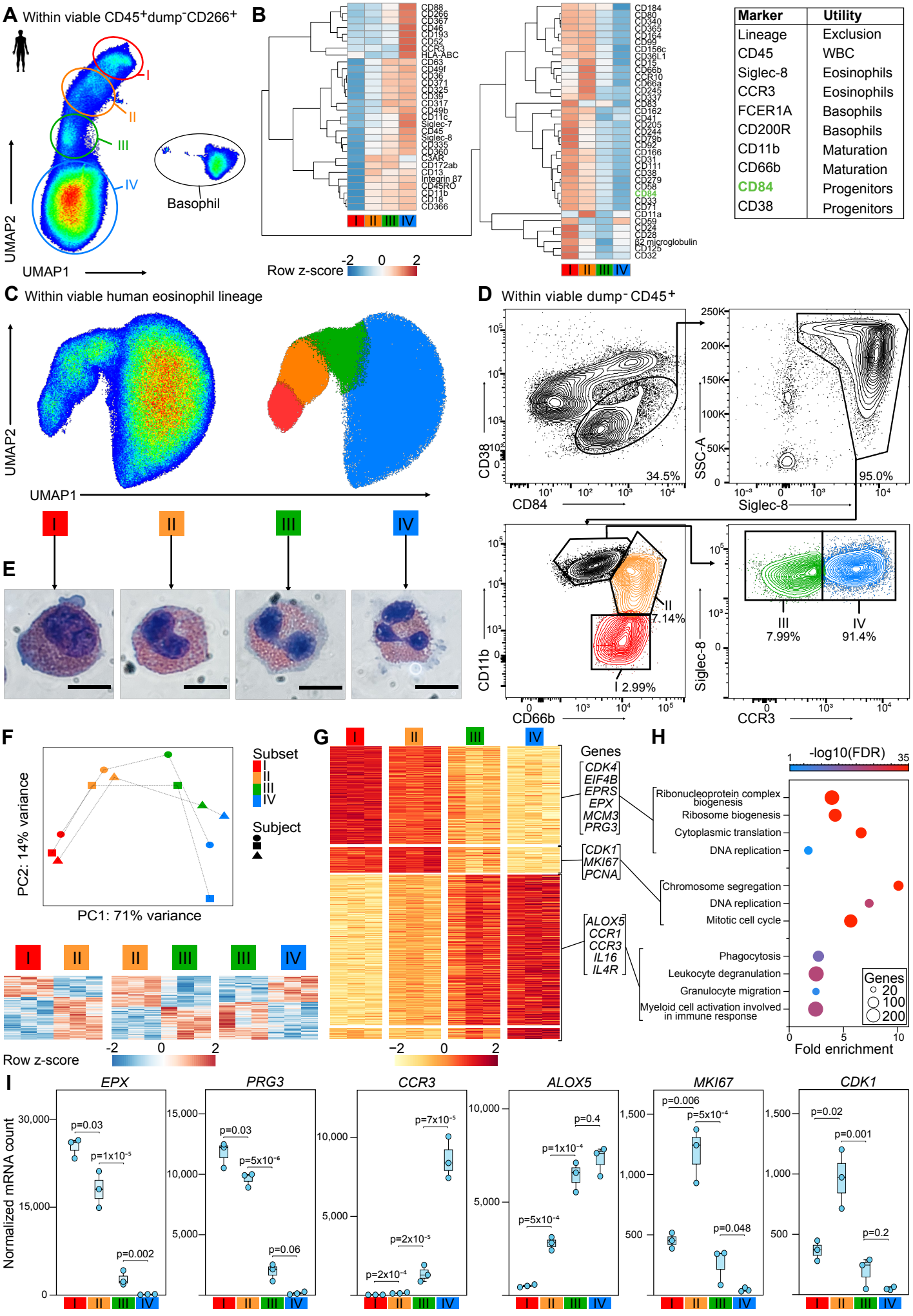
A Within viable CD45+dump-CD266+
UMAP2
UMAP1
I
II
III
IV
Basophil
B
CD88
CD266
CD367
CD46
CD193
CD52
CCR3
HLA-ABC
CD63
CD49f
CD36
CD371
CD325
CD39
CD317
CD49b
CD11c
Siglec-7
CD45
Siglec-8
CD335
CD360
C3AR
CD172ab
CD13
Integrin β7
CD45RO
CD11b
CD16
CD366
CD184
CD80
CD340
CD365
CD164
CD99
CD156c
CD96L1
CD15
CD66b
CCR10
CD66a
CD245
CD337
CD83
CD162
CD41
CD205
CD244
CD79b
CD92
CD166
CD31
CD111
CD38
CD279
CD58
CD84
CD33
CD71
CD11a
CD59
CD24
CD28
β2 microglobulin
CD125
CD32
I II III IV
-2 0 2
Row z-score
Marker | Utility
Lineage | Exclusion
CD45 | WBC
Siglec-8 | Eosinophils
CCR3 | Eosinophils
FCER1A | Basophils
CD200R | Basophils
CD11b | Maturation
CD66b | Maturation
CD84 | Progenitors
CD38 | Progenitors
C Within viable human eosinophil lineage
UMAP2
UMAP1
D Within viable dump- CD45+
CD38
CD84
34.5%
SSC-A
Siglec-8
95.0%
CD11b
CD66b
II 7.14%
I 2.99%
Siglec-8
CCR3
III 7.99%
IV 91.4%
E
I
II
III
IV
F
PC2: 14% variance
PC1: 71% variance
Subset
I
II
III
IV
Subject
I II
II III
III IV
-2 0 2
Row z-score
G
I II III IV
Genes
CDK4
EIF4B
EPRS
EPX
MCM3
PRG3
CDK1
MKI67
PCNA
ALOX5
CCR1
CCR3
IL16
IL4R
-2 0 2
H
-log10(FDR)
1 35
Ribonucleoprotein complex biogenesis
Ribosome biogenesis
Cytoplasmic translation
DNA replication
Chromosome segregation
DNA replication
Mitotic cell cycle
Phagocytosis
Leukocyte degranulation
Granulocyte migration
Myeloid cell activation involved in immune response
Genes
20
100
200
0 5 10
Fold enrichment
I
EPX
PRG3
CCR3
ALOX5
MKI67
CDK1
Normalized mRNA count
p=0.03
p=1x10-5
p=0.002
p=0.03
p=5x10-6
p=0.06
p=7x10-5
p=2x10-5
p=2x10-4
p=0.4
p=1x10-4
p=5x10-4
p=0.006
p=5x10-4
p=0.048
p=0.02
p=0.001
p=0.2
I II III IV

Figure 5

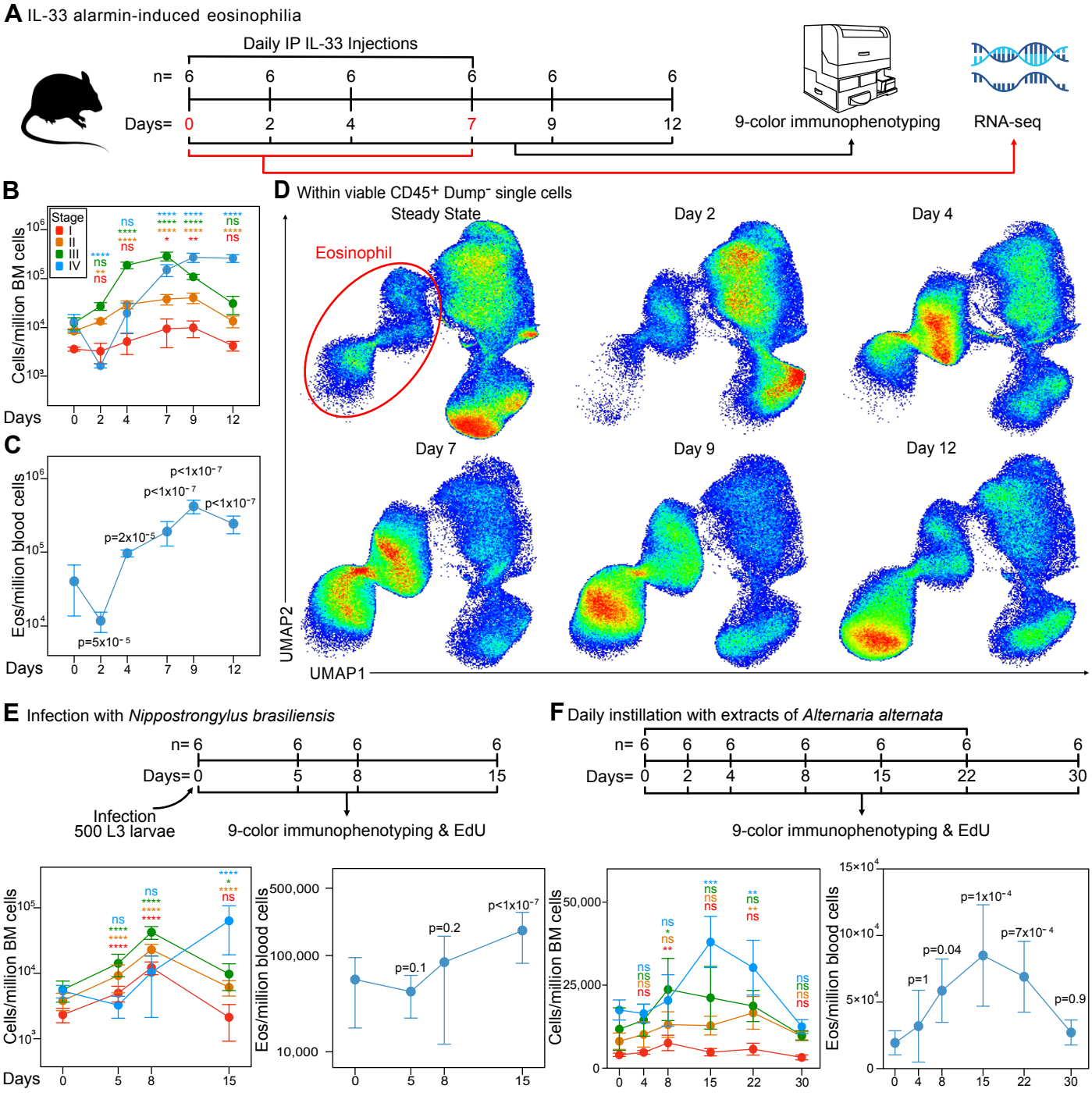
A IL-33 alarmin-induced eosinophilia
Daily IP IL-33 Injections
n= 6 6 6 6 6 6
Days= 0 2 4 7 9 12
9-color immunophenotyping
RNA-seq
B
Stage I II III IV
Cells/million BM cells
Days
C
Eos/million blood cells
p<1x10⁻⁷
p<1x10⁻⁷
p<1x10⁻⁷
p=2x10⁻⁵
p=5x10⁻⁵
Days
D Within viable CD45⁺ Dump⁻ single cells
Steady State
Eosinophil
Day 2
Day 4
Day 7
Day 9
Day 12
UMAP2
UMAP1
E Infection with Nippostrongylus brasiliensis
n= 6 6 6 6
Days= 0 5 8 15
Infection
500 L3 larvae
9-color immunophenotyping & EdU
Cells/million BM cells
Days
Eos/million blood cells
p=0.1
p=0.2
p<1x10⁻⁷
F Daily instillation with extracts of Alternaria alternata
n= 6 6 6 6 6 6 6
Days= 0 2 4 8 15 22 30
9-color immunophenotyping & EdU
Cells/million BM cells
Eos/million blood cells
p=1
p=0.04
p=1x10⁻⁴
p=7x10⁻⁴
p=0.9

Figure 6

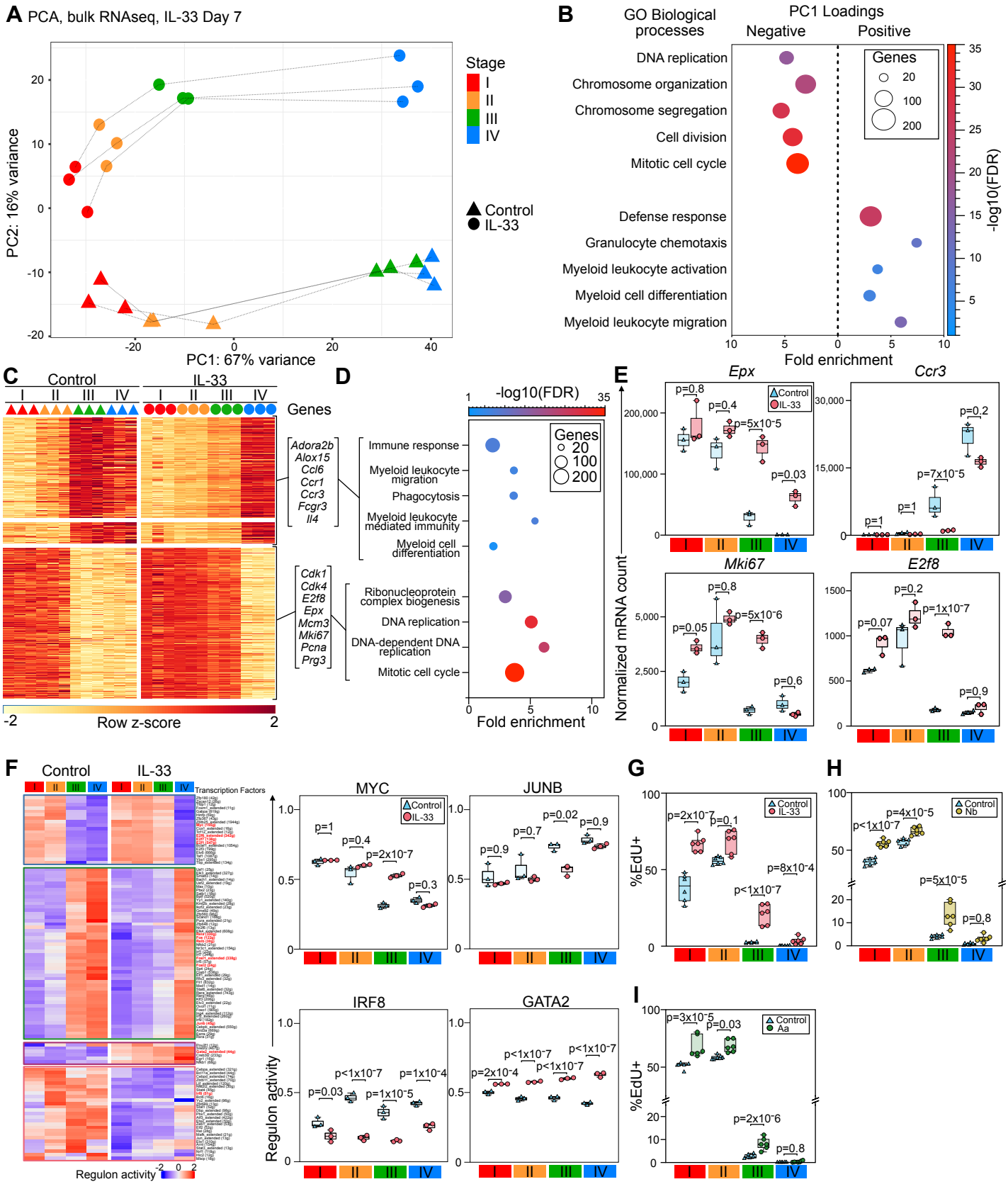
A PCA, bulk RNAseq, IL-33 Day 7
PC2: 16% variance
PC1: 67% variance
Stage
I
II
III
IV
Control
IL-33
B
GO Biological processes
PC1 Loadings
Negative
Positive
DNA replication
Chromosome organization
Chromosome segregation
Cell division
Mitotic cell cycle
Defense response
Granulocyte chemotaxis
Myeloid leukocyte activation
Myeloid cell differentiation
Myeloid leukocyte migration
Genes
20
100
200
-log10(FDR)
Fold enrichment
C
Control
IL-33
Genes
Adora2b
Alox15
Ccl6
Ccr1
Ccr3
Fcgr3
Il4
Cdk1
Cdk4
E2f8
Epx
Mcm3
Mki67
Pcna
Prg3
Row z-score
D
-log10(FDR)
Immune response
Myeloid leukocyte migration
Phagocytosis
Myeloid leukocyte mediated immunity
Myeloid cell differentiation
Ribonucleoprotein complex biogenesis
DNA replication
DNA-dependent DNA replication
Mitotic cell cycle
Fold enrichment
E
Epx
Ccr3
Mki67
E2f8
Control
IL-33
Normalized mRNA count
F
Control
IL-33
Transcription Factors
Regulon activity
MYC
JUNB
IRF8
GATA2
Regulon activity
G
%EdU+
Control
IL-33
H
%EdU+
Control
Nb
I
%EdU+
Control
Aa

Figure 7

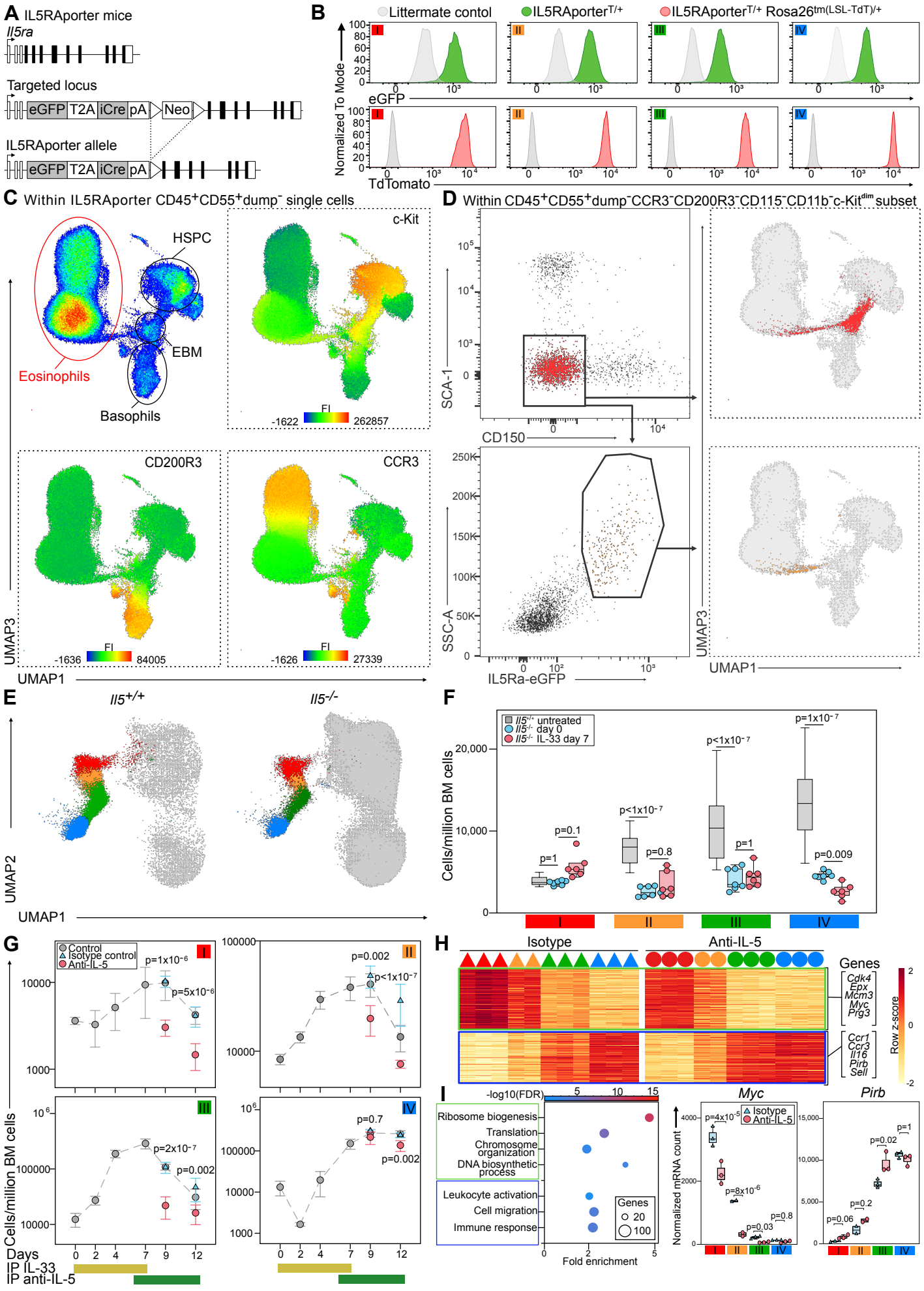
A IL5RAporter mice
Il5ra
Targeted locus
eGFP T2A iCre pA Neo
IL5RAporter allele
eGFP T2A iCre pA
B
Littermate contol
IL5RAporterT/+
IL5RAporterT/+ Rosa26tm(LSL-TdT)/+
Normalized To Mode
eGFP
TdTomato
C Within IL5RAporter CD45+CD55+dump- single cells
HSPC
EBM
Eosinophils
Basophils
c-Kit
CD200R3
CCR3
FI
-1622
262857
-1636
84005
-1626
27339
UMAP3
UMAP1
D Within CD45+CD55+dump-CCR3-CD200R3-CD115-CD11b-c-Kitdim subset
SCA-1
CD150
SSC-A
IL5Ra-eGFP
UMAP3
UMAP1
E
Il5+/+
Il5-/-
UMAP2
UMAP1
F
Il5+/+ untreated
Il5-/- day 0
Il5-/- IL-33 day 7
Cells/million BM cells
p=0.1
p=1
p<1x10-7
p=0.8
p<1x10-7
p=1
p=1x10-7
p=0.009
G
Control
Isotype control
Anti-IL-5
p=1x10-6
p=5x10-6
p=0.002
p<1x10-7
p=2x10-7
p=0.002
p=0.7
p=0.002
Cells/million BM cells
Days
IP IL-33
IP anti-IL-5
H
Isotype
Anti-IL-5
Genes
Cdk4
Epx
Mcm3
Myc
Prg3
Ccr1
Ccr3
Il16
Pirb
Sell
Row z-score
I
-log10(FDR)
Ribosome biogenesis
Translation
Chromosome organization
DNA biosynthetic process
Leukocyte activation
Cell migration
Immune response
Genes
20
100
Fold enrichment
Myc
Pirb
Normalized mRNA count
Isotype
Anti-IL-5
p=4x10-5
p=8x10-6
p=0.8
p=0.03
p=1
p=0.02
p=0.2
p=0.06

Supplemental Figures S1-S6

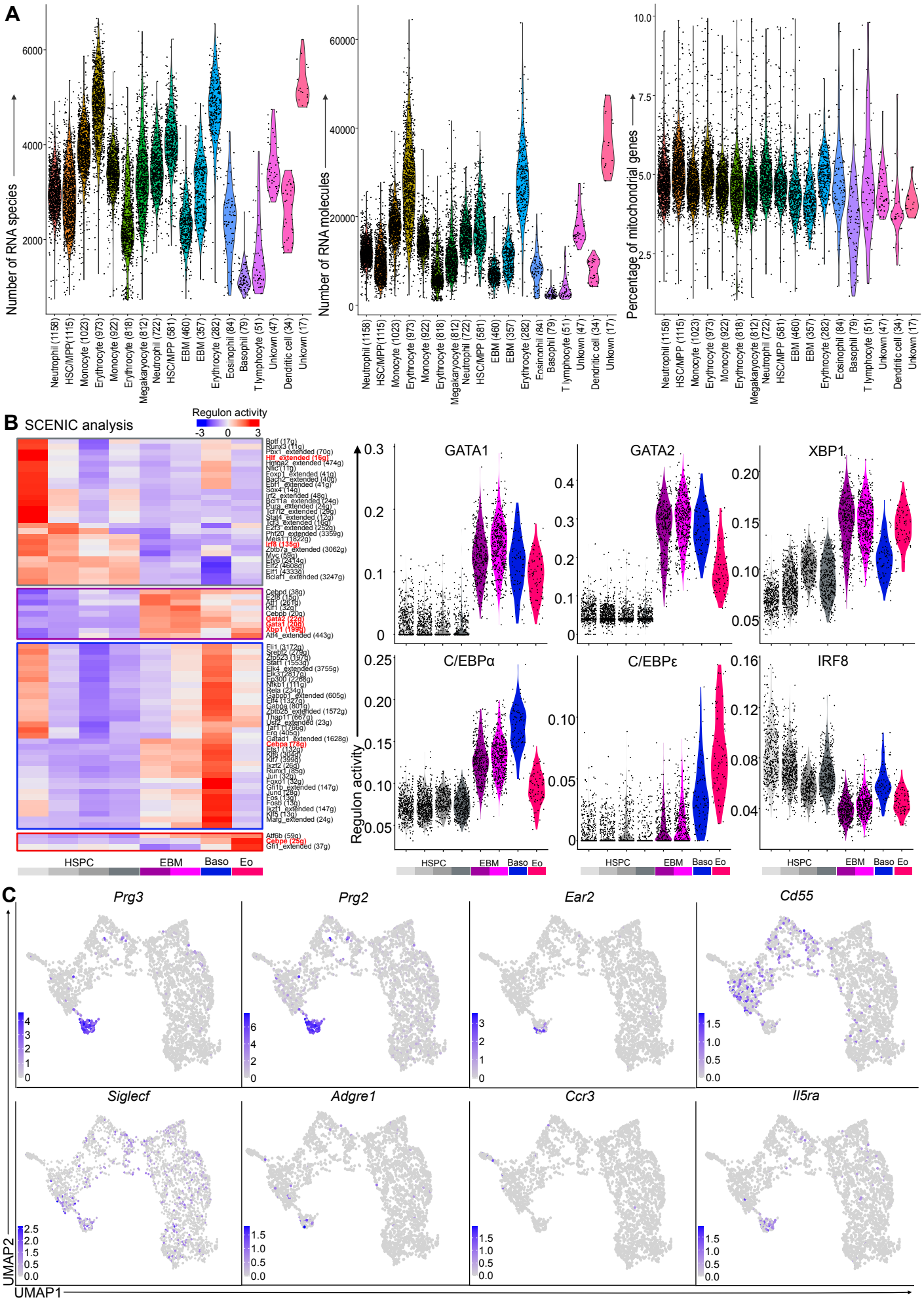

Figure S1. Single-cell RNA sequencing helps resolve murine eosinophil ontogeny, related to Figure 1. A. Violin plots of number of RNA species, number of RNA molecules, and percentage of mitochondrial genes in cell clusters of murine BM progenitors in Figure 1B. **B.** SCENIC analysis of cell clusters in Figure 1D presented as row-scaled heatmaps (left) or absolute activity of select regulons (right). **C.** Overlayed expression of eosinophil marker and cell surface marker genes on UMAP in Figure 1D. (Baso: basophil, EBM: eosinophil/basophil/mast cell progenitors, Eo: eosinophil, HSC/MPP: hematopoietic stem cell/multipotent progenitors)

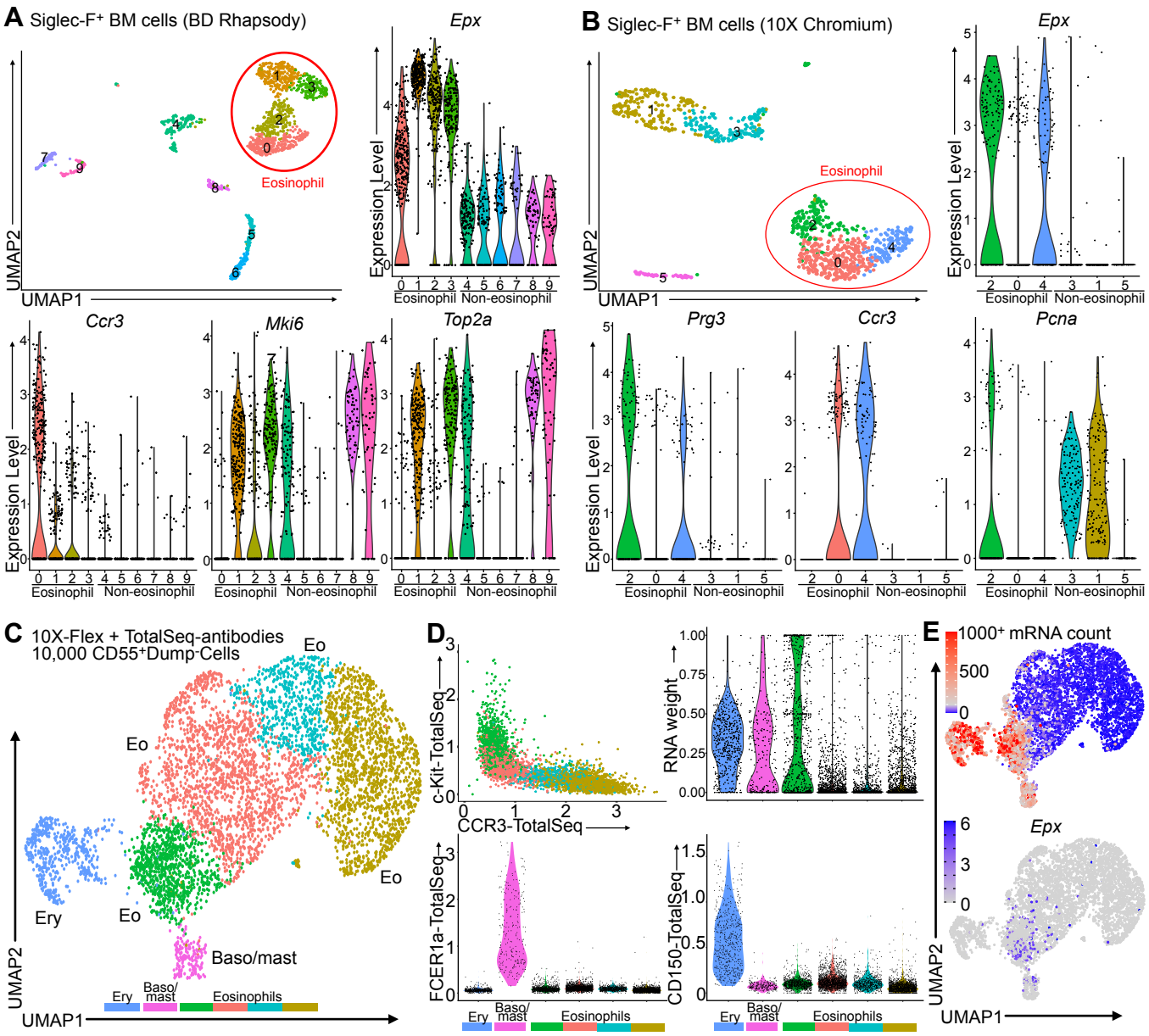

Figure S2. Single-cell RNA sequencing analysis of murine bone marrow using different platforms captures eosinophil lineage cells, related to Figure 1. A. UMAP with eosinophil lineage clusters highlighted in a reanalysis of SiglecF$^+$ BM cells from IL-5 transgenic mice in [8] using a resolution of 0.5 in Seurat, with violin plots of the indicated eosinophil marker and cell cycle-associated genes. **B.** UMAP with lineage annotation of a droplet-based scRNAseq analysis of SiglecF$^+$ BM cells from mice injected for 7 days with IL-33, with violin plots of expression probability distribution of the indicated eosinophil marker and cell cycle-associated genes. **C.** UMAP and lineage annotation of GATA1 lineage progenitors of steady-state murine BM in fixed droplet-based scRNAseq with oligo-antibody tags. **D.** Plot of c-Kit versus CCR3 oligo-tag antibody signal (upper left) and violin plots of RNA weight (upper right) and oligo-antibody tag signal (bottom) in cell clusters in C. **E.** Overlay of mRNA count (upper) and overlay of Epx mRNA signal (lower) in C. (Baso/mast: basophil/mast cell progenitor, Eo: eosinophil, Ery: erythroid)

A 13-color Backbone

Marker	Utility
CD45	Leukocytes
SCA-1	Stem cells
c-Kit	Progenitors
CD11b	Maturation
CD55	GATA1 lineages
CCR3	Mature Eos
Siglec-F	Mature Eos
CD200R3	Basophils
FcεR1α	Mast cells
CXCR2	Neutrophils
CD16/32	Neutrophils
CD115	Monocytes
Ly-6G	Dump
NK1.1	Dump
CD90.2	Dump
B220	Dump

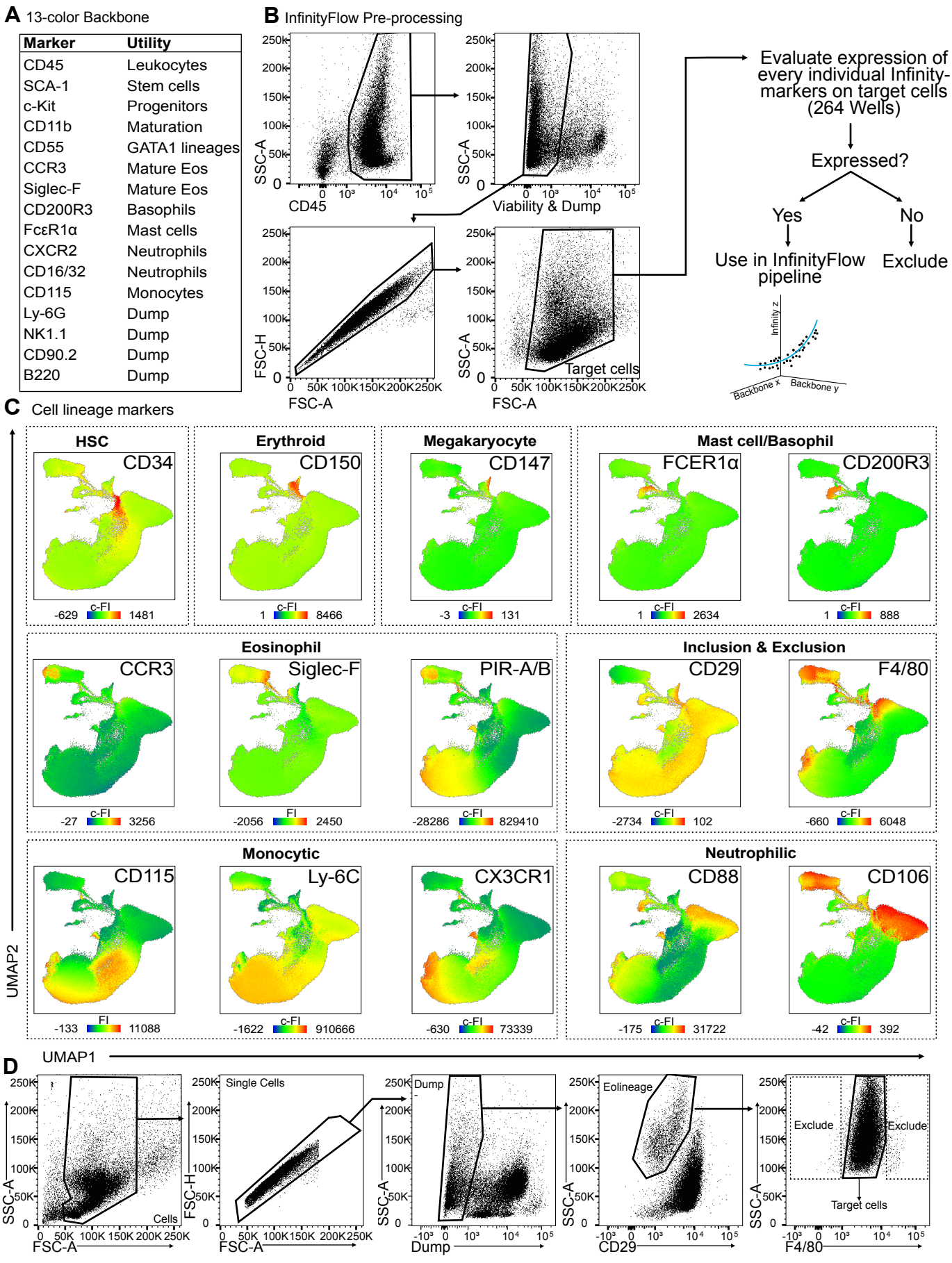

Figure S3. High dimension flow cytometric screening resolves murine eosinophilopoiesis, related to Figures 1 and 2. A. Backbone panel for flow cytometric screening of the murine eosinophil lineage. **B.** Gating strategy of murine bone marrow cells of interest and post-processing strategy for the inclusion of detected markers in the InfinityFlow computation. **C.** Overlayed staining intensity of lineage markers on the UMAP in Figure 1H. **D.** Gating strategy upstream of Figure 2D. (c-FI: background-corrected fluorescence intensity, Eos: eosinophil, FI: fluorescence intensity, HSC: hematopoietic stem cell).

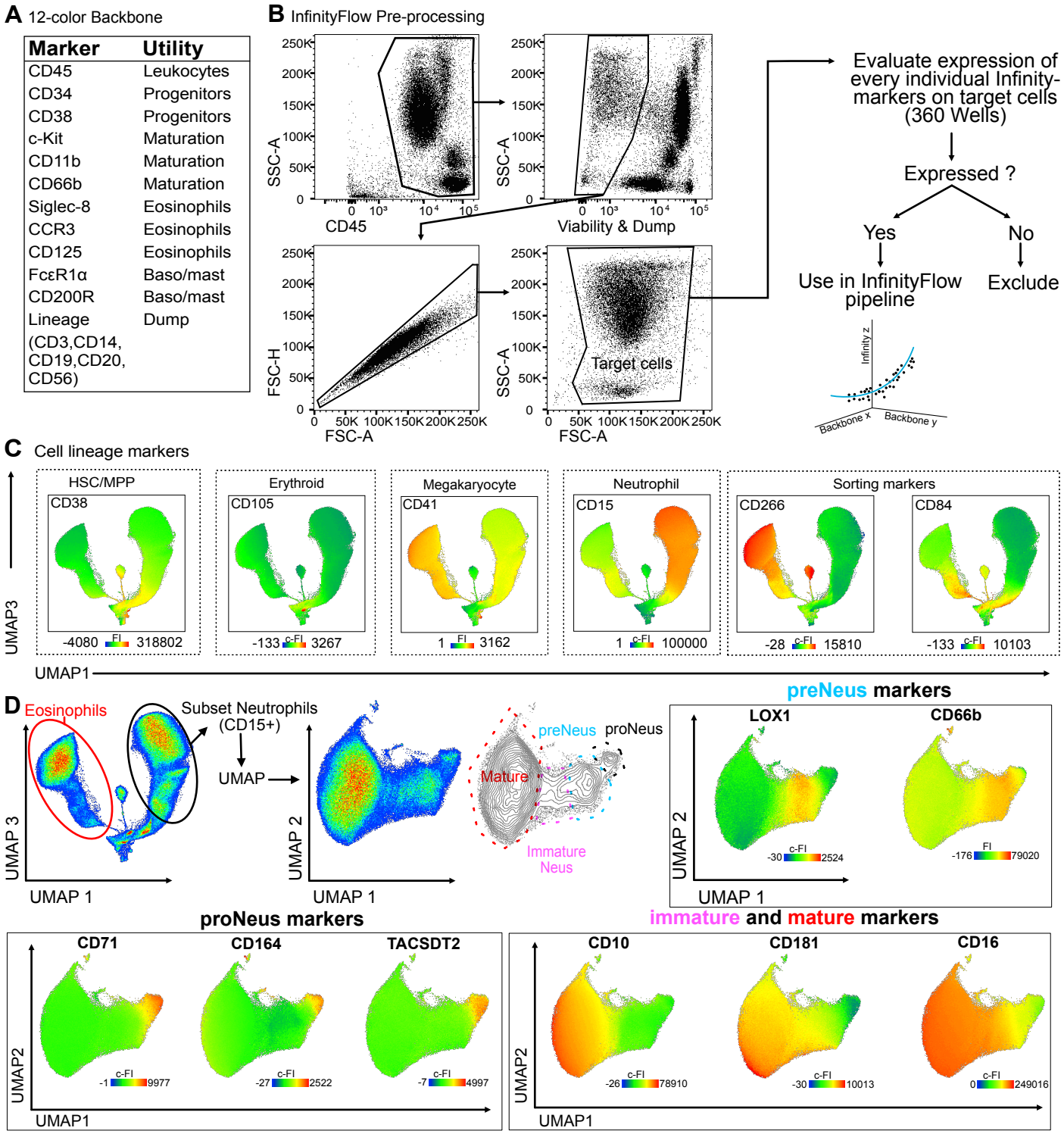

Figure S4. High dimension flow cytometric screening resolves human eosinophilopoiesis, related to Figure 3. **A.** Backbone panel for flow cytometric screening of the human eosinophil lineage. **B.** Gating strategy of human BM cells of interest and post-processing strategy for the inclusion of detected markers in the InfinityFlow computation. **C.** Overlayed staining intensity of lineage markers on the UMAP in Figure 3B. **D.** UMAP of neutrophil lineage cells subselected from Figure 3B and highlighting 4 previously described stages of neutrophil maturation [40] with overlayed expression of previously identified cell surface markers. (c-FI: background-corrected fluorescence intensity, FI: fluorescence intensity, HSC: hematopoietic stem cell, MPP: multipotent progenitor)

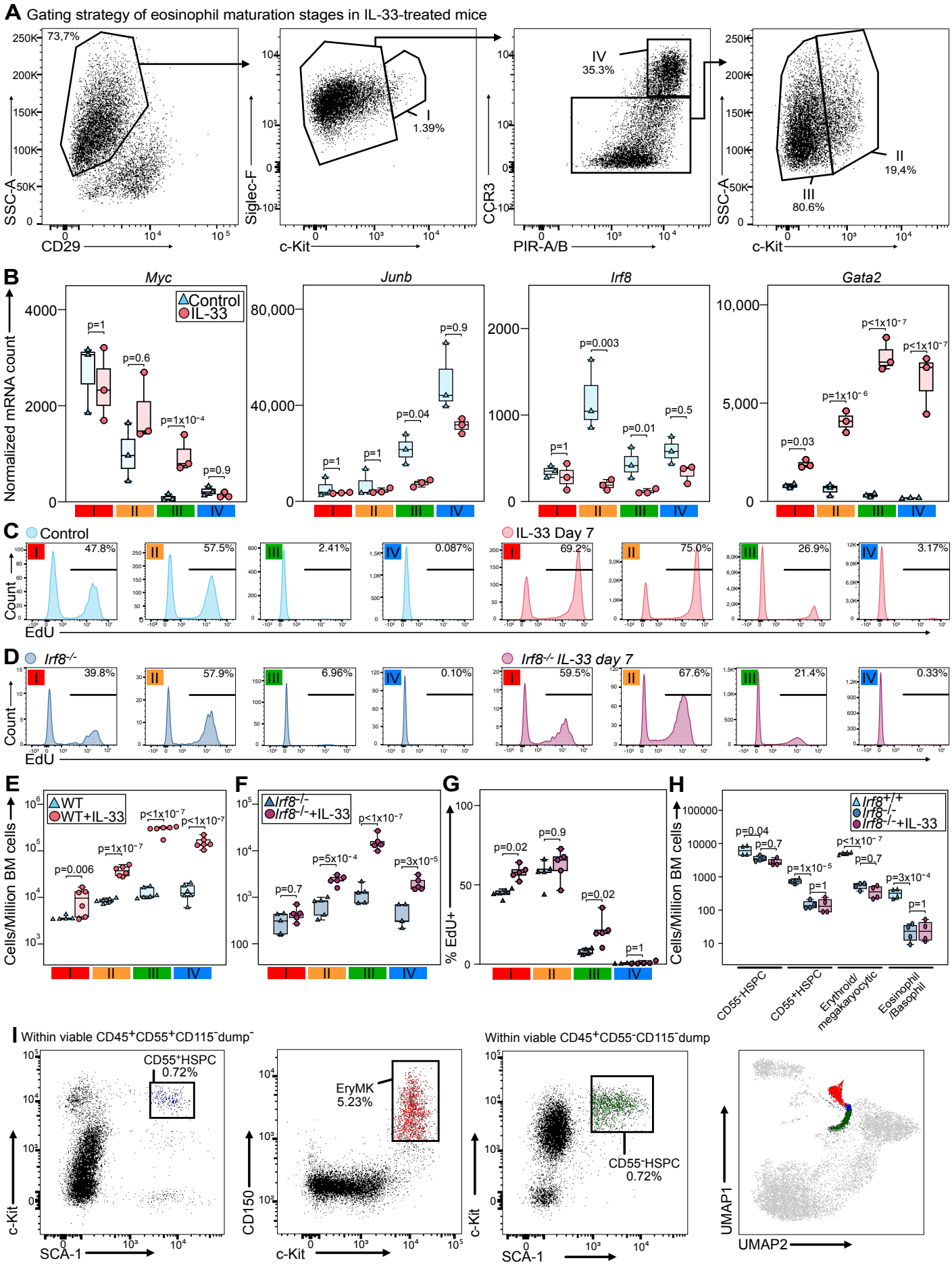
A Gating strategy of eosinophil maturation stages in IL-33-treated mice
73,7%
SSC-A
CD29
Siglec-F
c-Kit
I
1.39%
CCR3
PIR-A/B
IV
35.3%
II
19,4%
III
80.6%
B
Myc
Junb
Irf8
Gata2
Normalized mRNA count
Control
IL-33
p=1
p=0.6
p=1x10-4
p=0.9
p=0.04
p=0.003
p=0.01
p=0.5
p=0.03
p=1x10-6
p<1x10-7
C
Control
IL-33 Day 7
Count
EdU
47.8%
57.5%
2.41%
0.087%
69.2%
75.0%
26.9%
3.17%
D
Irf8-/-
Irf8-/- IL-33 day 7
39.8%
57.9%
6.96%
0.10%
59.5%
67.6%
21.4%
0.33%
E
WT
WT+IL-33
Cells/Million BM cells
p=0.006
p=1x10-7
p<1x10-7
F
Irf8-/-
Irf8-/-+IL-33
p=0.7
p=5x10-4
p=3x10-5
G
% EdU+
p=0.02
p=0.9
H
Irf8+/+
Irf8-/-
Irf8-/-+IL-33
p=0.04
p=0.7
p=1x10-5
p=1
p<1x10-7
p=3x10-4
CD55+HSPC
CD55+HSPC
Erythroid/ megakaryocytic
Eosinophil /Basophil
I Within viable CD45+CD55+CD115-dump-
CD55+HSPC
0.72%
c-Kit
SCA-1
EryMK
5.23%
CD150
Within viable CD45+CD55-CD115-dump
CD55-HSPC
0.72%
UMAP1
UMAP2

Figure S5. Cell cycling activity of eosinophil progenitors increases in eosinophilic conditions, related to Figures 5 and 6. A. Gating strategy of the 4 maturation stages of eosinophils in the BM of mice treated with recombinant IL-33 i.p. for 7 days. Compare with Figure 2D. **B.** Comparison of normalized gene expression of selected transcription factors in Figure 6F (n=3/group). **C-D**. Representative flow cytometric histograms of the incorporation of EdU after a 1h pulse in stage I-IV progenitors of control mice, mice treated with recombinant IL-33 for 7 days (C), or *Irf8*$^{-/-}$ mice treated or not with IL-33 for 7 days (D). **E-F.** Comparison of the abundance of stage I-IV eosinophils in the bone marrow of *Irf8*$^{-/-}$ mice (E) or wild-type (WT) mice (E, data from Figure 5B) treated or not with IL-33 for 7 days (n=5-6/group, pooled from 2 independent experiments). **G.** Comparison of 5-ethynyl-2'-deoxyuridine (EdU) incorporation after a 1h pulse in mice in (F). **H.** Comparison of the abundance of CD55^{-} and CD55^{+} HSPCs (Dump^{-} Sca1^{+} c-Kit^{+}), erythroid/megakaryocytic progenitors (Dump^{-} Sca1^{-} c-Kit^{+} CD150^{+}) and eosinophil/basophil progenitors in mice in (G) (box-and-whisker diagrams with minimum and maximum values as boundaries, one-way ANOVA followed by TukeyHSD post-hoc tests for each cell subset). **I.** Gating strategy of cell populations in (H). (B, E-G: box-and-whisker diagrams with minimum and maximum values as boundaries, 2-way ANOVA followed by TukeyHSD post-hoc tests)

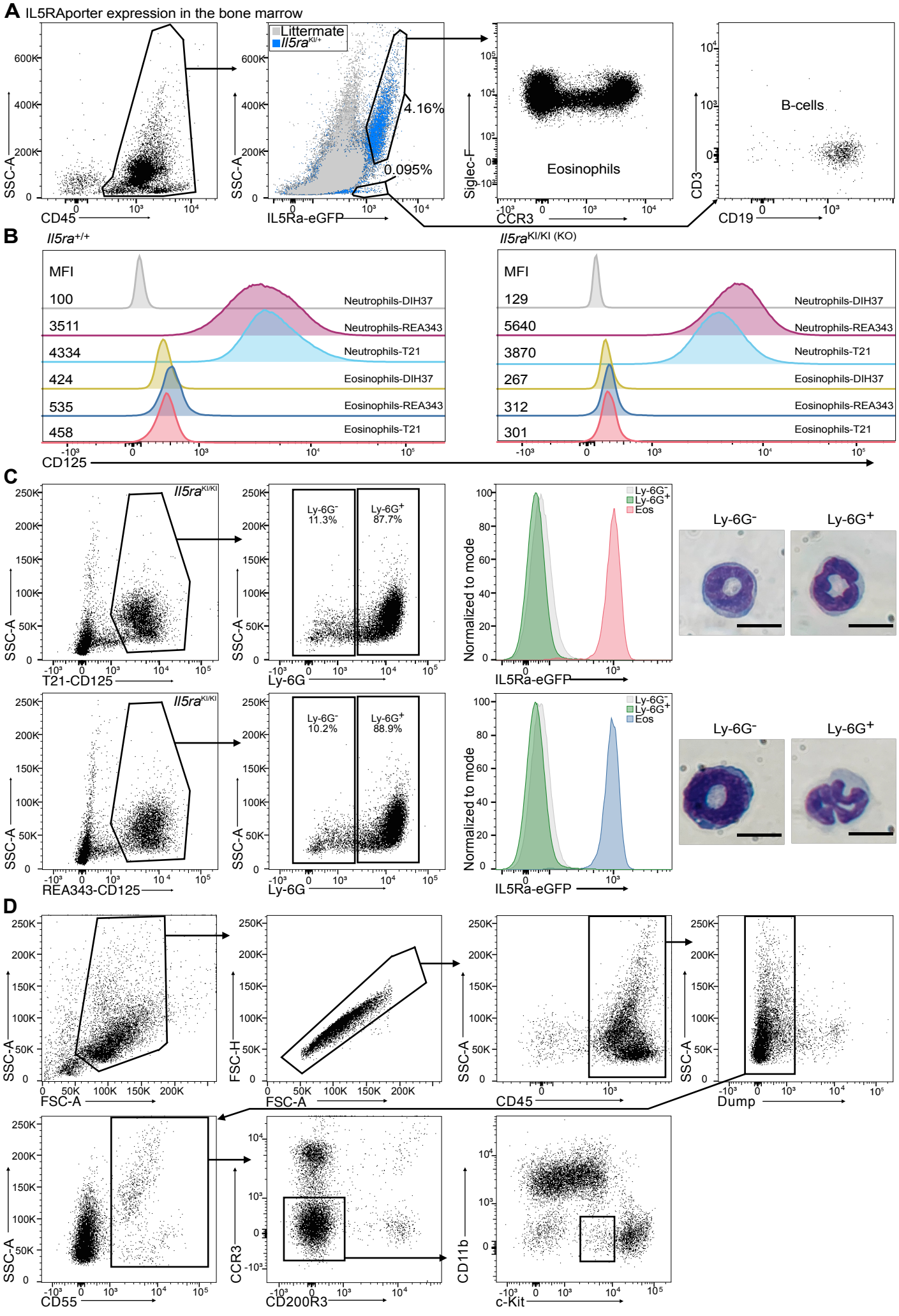
A IL5RAporter expression in the bone marrow
SSC-A
CD45
Littermate
Il5ra KI/+
IL5Ra-eGFP
4.16%
0.095%
Siglec-F
CCR3
Eosinophils
CD3
CD19
B-cells
B
Il5ra+/+
Il5ra KI/KI (KO)
MFI
100
Neutrophils-DIH37
3511
Neutrophils-REA343
4334
Neutrophils-T21
424
Eosinophils-DIH37
535
Eosinophils-REA343
458
Eosinophils-T21
CD125
129
5640
3870
267
312
301
C
Il5ra KI/KI
T21-CD125
Ly-6G
Ly-6G- 11.3%
Ly-6G+ 87.7%
Normalized to mode
Ly-6G-
Ly-6G+
Eos
IL5Ra-eGFP
REA343-CD125
Ly-6G- 10.2%
Ly-6G+ 88.9%
D
FSC-A
FSC-H
CD45
Dump
CD55
CCR3
CD200R3
CD11b
c-Kit

Figure S6. IL-5Rα reporter mice identify *bona fide Il5ra*-expressing cells, related to Figure 7. A. Representative gating strategy in flow cytometry of $eGFP^+$ eosinophils and of a subset of B cells in the BM of $IL5RAporter^{KI/+}$ mice. Overlay with a littermate wild-type sample is provided for comparison. **B.** Representative flow cytometric histograms of staining with anti-CD125 antibody clones DIH37, REA343 and T21 of neutrophils and eosinophils of wild-type (left) and *Il5ra*-deficient $IL5RAporter^{KI/KI}$ mice (right). **C.** Representative gating strategy in flow cytometry of cells staining brightly with anti-CD125 antibody clones T21 and REA343, comparison with eGFP reporter fluorescence intensity of eosinophils in $IL5RAporter^{KI/KI}$ mice, and light microscopic pictures of $Ly6G^-$ and $Ly6G^+$ cells brightly staining with T21 or RE343 showing their neutrophilic identity (scale bar: 10µm). **D.** Gating strategy of eosinophil/basophil progenitors upstream of Figure 7D, as in Figure 1K. (Eos: eosinophil, KI: knock-in, KO: knockout).

Supplemental Table 3

Table S3. Markers of murine cell populations of interest in Figure 1H (upper) and of human cell populations of interest in Figure 3B (lower)

Cell lineage	**Markers**
Murine	
HSC/MPP	CD117, CD135, CD34, Sca-1
Megakaryocyte	CD55, CD117, CD150, CD105, CD147
Erythroid	CD55, CD117, CD105, CD150
Basophil/mast cell	CD55, CD200R3, FcεR1α
Mast cell	CD55, Integrin β7, CD117, FcεR1α
Eosinophil	CD55, CD11b, CCR3, F4/80, PIR-A/B, Siglec-F
Monocyte	CD11b, CD115, CX3CR1, Ly-6C
Neutrophil	CD11b, Ly-6G/Ly-6C, CD88, CD106
B cell	CD138, CD19, CD20, CD2, CD5
Human	
HSC/MPP	CD34, CD38
Erythroid	CD36, CD105
Basophil	CD200R, CD193, CD123
Mast cell	CD203C, CD117, FcεR1α
Eosinophil	CD11b, CD193, Siglec-8, CD125
Monocyte	CD11b, CD192, CD172ab
Neutrophil	CD15, CD11b